Title

OFCD syndrome and extraembryonic defects are revealed by conditional mutation of the Polycomb-group repressive complex 1.1 (PRC1.1) gene BCOR

Journal

Developmental Biology, 468(1-2)

ISSN

0012-1606

Authors

Hamline, Michelle Y
Corcoran, Connie M
Wamstad, Joseph A
et al.

Publication Date

2020-12-01

DOI

10.1016/j.ydbio.2020.06.013

Peer reviewed

HHS Public Access

Author manuscript

Dev Biol. Author manuscript; available in PMC 2022 October 20.

Published in final edited form as:

Dev Biol. 2020 December 01; 468(1-2): 110–132. doi:10.1016/j.ydbio.2020.06.013.

OFCD Syndrome and Extraembryonic Defects are Revealed by Conditional Mutation of the Polycomb-group Repressive Complex 1.1 (PRC1.1) Gene *Bcor*

Michelle Y. Hamline[a,b,1,2], **Connie M. Corcoran**[c,1], **Joseph A. Wamstad**[a,3], **Isabelle Miletich**[d], **Jifan Feng**[d,4], **Jamie L. Lohr**[e], **Myriam Hemberger**[f], **Paul T. Sharpe**[d,g], **Micah D. Gearhart**[c,d,*], **Vivian J. Bardwell**[c,h,i,*]

[a]The Molecular, Cellular, Developmental Biology and Genetics Graduate Program, University of Minnesota, Minneapolis, MN 55455, USA

[b]University of Minnesota Medical Scientist Training Program, University of Minnesota, Minneapolis, MN 55455, USA

[c]Department of Genetics, Cell Biology and Development, University of Minnesota, Minneapolis, MN 55455, USA

[d]Centre for Craniofacial and Regenerative Biology, Faculty of Dentistry, Oral and Craniofacial Sciences, King's College London, London SE1 9RT, UK

[e]Department of Pediatrics, University of Minnesota, Minneapolis, MN 55455, USA

[f]Department of Biochemistry and Molecular Biology, Alberta Children's Hospital Research Institute, Cumming School of Medicine, University of Calgary, Calgary, AB University of Calgary

[g]MRC Centre for Transplantation, King's College London, London, SE1 9RT UK

[h]Developmental Biology Center, University of Minnesota, Minneapolis, MN 55455, USA

[i]Masonic Cancer Center, University of Minnesota, Minneapolis, MN 55455, USA

Abstract

BCOR is a critical regulator of human development. Heterozygous mutations of *BCOR* in females cause the X-linked developmental disorder Oculofaciocardiodental syndrome (OFCD), and hemizygous mutations of *BCOR* in males cause gestational lethality. BCOR associates with Polycomb group proteins to form one subfamily of the diverse Polycomb repressive complex 1 (PRC1) complexes, designated PRC1.1. Currently there is limited understanding of differing developmental roles of the various PRC1 complexes. We therefore generated a conditional exon 9–10 knockout *Bcor* allele and a transgenic conditional *Bcor* expression allele and used these to define multiple roles of *Bcor*, and by implication PRC1.1, in mouse development. Females

*Corresponding authors: 6-160 Jackson Hall, 321 Church St SE, Minneapolis, MN 55455, bardw001@umn.edu, Telephone: 1-612-626-7028, gearh006@umn.edu, Telephone: 1-612-626-4844, Fax: 1-612-626-6140.

[1]These author contributed equally to this work

[2]Present address: Department of Pediatrics, University of California Davis Health, Sacramento, CA 95817, USA

[3]Present address: Novartis Institutes for BioMedical Research, Cambridge, MA 02139, USA

[4]Present address: Center for Craniofacial Molecular Biology, Ostrow School of Dentistry of University of Southern California, Los Angeles, CA 90033, USA

heterozygous for *Bcor* exhibiting mosaic expression due to the X-linkage of the gene showed reduced postnatal viability and had OFCD-like defects. By contrast, *Bcor* hemizygosity in the entire male embryo resulted in embryonic lethality by E9.5. We further dissected the roles of *Bcor*, focusing on some of the tissues affected in OFCD through use of cell type specific *Cre* alleles. Mutation of *Bcor* in neural crest cells caused cleft palate, shortening of the mandible and tympanic bone, ectopic salivary glands and abnormal tongue musculature. We found that defects in the mandibular region, rather than in the palate itself, led to palatal clefting. Mutation of *Bcor* in hindlimb progenitor cells of the lateral mesoderm resulted in 2/3 syndactyly. Mutation of *Bcor* in *Isl1*-expressing lineages that contribute to the heart caused defects including persistent truncus arteriosus, ventricular septal defect and fetal lethality. Mutation of *Bcor* in extraembryonic lineages resulted in placental defects and midgestation lethality. Ubiquitous over expression of transgenic *Bcor* isoform A during development resulted in embryonic defects and midgestation lethality. The defects we have found in *Bcor* mutants provide insights into the etiology of the OFCD syndrome and how BCOR-containing PRC1 complexes function in development.

Keywords

Oculofaciocardiodental syndrome; craniofacial; cardiac; X-linked developmental disorder; salivary glands; placenta

Introduction

Development is driven by specific spatial and temporal patterns of gene expression. The Polycomb system, a major gene silencing system found in all metazoans, is important for orchestrating these patterns of gene expression (Aloia et al., 2013; Schuettengruber et al., 2017). In vertebrates there are two key classes of Polycomb complexes, Polycomb-group Repressive Complex 1 and 2 (PRC1 and PRC2) (Schuettengruber et al., 2017; Simon and Kingston, 2013). There is increasing appreciation that duplication and divergence of the genes encoding PRC1 components has led to multiple PRC1 complexes whose precise compositions are thought to vary by developmental stage and/or cell type (Gao et al., 2012; Kerppola, 2009; Luis et al., 2012; Trojer et al., 2011; Vidal and Starowicz, 2017). It is now evident that these complexes have different functions and targets and thus will control specific aspects of growth and development (Connelly and Dykhuizen, 2017; Di Carlo et al., 2019; Endoh et al., 2017; Gil and O'Loghlen, 2014). All PRC1 complexes described so far contain an enzymatic core consisting of RING1(RING1A) or RNF2 (RING1B), which ubiquitylates H2A, and a PCGF component (Elderkin et al., 2007; Gao et al., 2012; Gearhart et al., 2006; Levine et al., 2002; Ogawa et al., 2002; Wang et al., 2004) that stimulates this ubiquitylation (Buchwald et al., 2006; Cao et al., 2005; Wu et al., 2008). There are at least six different families of PRC1 complexes, classified based on which PCGF component is present.

We previously identified BCOR through its interaction with the transcription factor and oncoprotein BCL6 (Huynh et al., 2000). We subsequently found that BCOR is a component of a non-canonical PRC1 complex that also contains KDM2B (Gearhart et al., 2006), a protein that can demethylate H3K36 (He et al., 2008) and has a CXXC domain that binds

non-methylated CpG nucleotides helping to target PRC1 complexes to DNA (Farcas et al., 2012; He et al., 2013; Wu et al., 2013). BCOR is a central component of PRC1.1 complexes with a RING1/RNF2:PCGF1 core (Gao et al., 2012; Gearhart et al., 2006; Junco et al., 2013; Sanchez et al., 2007) although interactions between BCOR and PCGF3 have also been observed (Gao et al., 2012; Gearhart et al., 2006; Junco et al., 2013; Sanchez et al., 2007). Since BCOR is only found in a subset of PRC1 complexes, dissection of its specific functions in development should provide insights into the functional specialization of PRC1.1, a non-canonical PRC1. Furthermore, BCOR is of clinical interest because human mutations and *in vivo* and *in vitro* studies have indicated that it plays important roles in cancer and development.

BCOR is a mediator of BCL6 function and thus is likely important in BCL6-driven cancers (Beguelin et al., 2016; Gearhart et al., 2006; Ghetu et al., 2008; Hatzi et al., 2013; Huynh et al., 2000). The occurrence of in-frame internal *BCOR* tandem duplications in clear cell sarcoma of the kidney and at least two other types of cancer, together with translocations generating BCOR fusion proteins in Ewing-like sarcomas indicate that mutations involving *BCOR* may be oncogenic (Astolfi et al., 2015; Pierron et al., 2012; Roy et al., 2015; Specht et al., 2016; Ueno-Yokohata et al., 2015; Yoshida et al., 2018). In contrast, analysis of patient tumor DNA in other cancer types suggests that BCOR also can act as a tumor suppressor (Damm et al., 2013; Grossmann et al., 2011; Herold et al., 2014; Pugh et al., 2012; Seki et al., 2015; Yamamoto et al., 2014; Yan et al., 2012; Yoshida et al., 2011; Zhang et al., 2012), where it may function independently of BCL6.

BCOR also plays an essential role in human development. Mutations in *BCOR* result in two rare X-linked Microphthalmia Syndromic 2 (MCOPS2) disorders: Oculofaciocardiodental Syndrome (OFCD) and MAA2 associated Lenz microphthalmia (Ng et al., 2004). The recognition of OFCD began when Robert Gorlin (Marashi and Gorlin, 1990) suggested that congenital cataracts linked with radiculomegaly (extended root growth) of canine teeth constitutes a syndrome. Further characterization led to the definition of OFCD (formally syndromic microphthalmia 2; MCOPS2) (Obwegeser and Gorlin, 1997; Wilkie et al., 1993), in which female OFCD patients can have defects in the craniofacial, skeletal, and cardiovascular systems. Fewer than 100 OFCD patients have been described and all are heterozygous for a mutant *BCOR* allele (Feberwee et al., 2014; Hilton et al., 2008; Hilton et al., 2009; Ragge et al., 2018). While mother-to-daughter transmission of the disease has been reported (Hilton et al., 2008; Horn et al., 2005; Ng et al., 2004), no male OFCD patients have been observed, strongly suggesting that hemizygosity for *BCOR* mutations results in embryonic lethality (Ng et al., 2004). Virtually all reported OFCD mutations, which include nonsense, frameshifting insertions/deletions/duplications, splicing mutations, and large deletions (Fig. 1A), are predicted to reduce *BCOR* function via gene loss or protein truncation and/or nonsense-mediated decay (Danda et al., 2014; Di Stefano et al., 2015; Feberwee et al., 2014; Hilton et al., 2008; Hilton et al., 2009; Ma et al., 2016; Ng et al., 2004; Ragge et al., 2018; Surapornsawasd et al., 2014; Zhou et al., 2017).

In females, the severity of the OFCD syndrome differs considerably from patient to patient (Feberwee et al., 2014; Hilton et al., 2008; Hilton et al., 2009; Ragge et al., 2018). BCOR is X-linked, and X chromosome inactivation (XCI) occurs randomly in the early embryo.

As a consequence, the variable range and severity of phenotypes between individuals likely reflects individual variation within key tissues in the proportion of cells that have a transcriptionally active X chromosome containing the *BCOR* mutation. Alternatively, a phenotype may not be apparent if cells with the *BCOR* mutation on the active X chromosome do not survive. This was seen with X-inactivation analyses of leukocytes from OFCD patients, which displayed 96–100% allelic skewing in favor of cells expressing the wild type allele of *BCOR* (Hedera and Gorski, 2003; Ng et al., 2004).

Female OFCD patients commonly display a distinctive craniofacial phenotype including radiculomegaly and other dental abnormalities, cataracts, midfacial hypoplasia, and a long narrow face but with a characteristic broad or bifid nose. In addition, cleft palate or a high arched palate occurs in over a quarter of patients and is sometimes associated with bifurcation of the uvula and tongue. Mandibular asymmetry and either a small or prominent mandible also occur. Other defects of the craniofacial region are found with variable penetrance; patients occasionally have macrocephaly (large head) or microcephaly (small head). Patients may also have abnormalities of ear structure, and 9% of patients have mild conductive or sensorineural hearing loss. OFCD skeletal defects include limb defects, which are generally found at lower incidence than the craniofacial defects and mainly include flexion deformities of the toes (“hammer toes”), toe syndactyly, and radioulnar synostosis (Feberwee et al., 2014; Hilton et al., 2008; Hilton et al., 2009; Ng et al., 2004; Ragge et al., 2018; Suzumori et al., 2013). Of the OFCD patients in whom cardiac function has been studied, 67% have at least one cardiovascular defect. Although the specific defects vary, septal defects (atrial, ventricular, or both) are the most common and are found in 50% of OFCD patients examined. Other cardiovascular defects observed include patent ductus arteriosus (6%) and double outlet right ventricle (3%) (Hilton et al., 2009; Ragge et al., 2018).

MAA2 associated Lenz Microphthalmia presentation is characterized by microphthalmia and clinical anophthalmia, mental retardation, cardiac anomalies, radioulnar synostosis, and other skeletal anomalies and results from a *BCOR* missense point mutation (P85L). This mutation has been clinically confirmed in six males to date (Hilton et al., 2009; Ng et al., 2004; Ragge et al., 2018; Suzumori et al., 2013). More recently different point mutations (R540Q, D551N and S1603R) have been reported in *BCOR* in male patients with symptoms suggestive of some features of Lenz Microphthalmia/OFCD syndromes (Du et al., 2018; Ragge et al., 2018; Zhu et al., 2015b).

In adult mice, *Bcor* is widely expressed (Huynh et al., 2000; Wamstad and Bardwell, 2007) but is dynamic throughout development with expression often paralleling the affected tissues in human OFCD patients (Cai et al., 2010; Wamstad and Bardwell, 2007). Early in development, *Bcor* is expressed most strongly in extraembryonic tissue but also in the neural folds, branchial arches and tail bud, and by embryonic day 9.5 (E9.5), expression is more widespread, with stronger expression detected in the branchial arches, limb buds, and neural tube. By E13.5, *Bcor* is expressed at low levels throughout much of the embryo proper, with higher levels in the neural tube, olfactory epithelium, teeth primordia, retina, and lens of the eye (Wamstad and Bardwell, 2007). *Bcor* also is expressed in the embryonic maxilla and mandible. From E11.5 to 14.5, *Bcor* is strongly expressed in the tongue and mandibular

tooth primordia. At E13.5, *Bcor* is expressed at the medial edge epithelium (MEE) of the palatal shelves, and at E14.5, in the palatal rugae and MEE fusion as well as the whisker primordia (Cai et al., 2010).

Animal studies have begun to examine the functions of *Bcor* in embryonic development. In zebrafish and *Xenopus*, morpholino inhibition of *Bcor* partially recapitulated the disease phenotype present in human OFCD patients (Hilton et al., 2007; Ng et al., 2004). In zebrafish, this inhibition resulted in developmental perturbations of the eye, skeleton, and central nervous system (Ng et al., 2004). In *Xenopus* early embryos, anti-*Bcor* morpholino treatment caused OFCD-related eye phenotypes, including colobomas, microphthalmia, and optic nerve irregularities (Hilton et al., 2007). Additionally, unilateral morpholino injections revealed that left sided knock down of *xtBcor* induced laterality defects in the gut and heart. Furthermore in *Xenopus*, BCOR blocks the transcription of selected NOTCH target genes to maintain left right asymmetry (Sakano et al., 2010; Tanaka et al., 2014). These results are consistent with clinical evidence reporting a subset of OFCD patients with dextrocardia, asplenia, and intestinal malrotation (Hedera and Gorski, 2003; Hilton et al., 2007).

Two laboratories have previously performed global *Bcor* knockout studies in mice, but because the animals could not be propagated, extensive developmental studies were not possible. In the first study (Wamstad et al., 2008), we generated a hypomorphic $Bcor^{Neo}$ allele. Female $Bcor^{Neo/+}$ mice had OFCD-related hematopoietic and ocular developmental abnormalities including a higher incidence of lens opacification, indicative of a propensity to develop cataracts. These heterozygous mice also failed to transmit the mutant allele to their offspring; this represented a strong parent-of-origin effect, as male chimeras with the $Bcor^{Neo}$ allele successfully transmitted the allele. In mice, the paternal X-chromosome is inactivated in extraembryonic tissues and *Bcor* is expressed at high levels in these tissues (Wamstad and Bardwell, 2007). Thus, a possible explanation for the parent-of-origin effect is that a functional *Bcor* allele is required in extraembryonic tissues, and therefore the *Bcor* mutant X chromosome cannot be maternally-derived. In a second study (Cox et al., 2010), as part of a large mutational screen of X-linked genes, gene trap embryonic stem (ES) cell lines targeting *Bcor* were aggregated with wild-type embryos to generate ES cell-derived embryos for phenotypic analysis. Two independent lines showed lethality by E9.5 with apparent fusion of the ventral forebrain, greatly reduced and malformed cardiac tissue, and severe posterior truncation with failure of chorioallantoic fusion. A third line was also lethal but had a somewhat less severe phenotype. Together these mouse studies highlighted the importance of *Bcor* in development but were limited in scope due to the inability to propagate these alleles.

Here, to examine the role of *Bcor* in development in greater depth and with cell-type specificity, we have generated two conditional *Bcor* alleles, one that mimics the loss-of-function mutation observed in human patients with OFCD, and one designed to overexpress *Bcor.* These studies further our understanding of the developmental basis of OFCD and may eventually aid the diagnosis and treatment of affected individuals.

Materials and Methods

Animal care

Mice were maintained in conventional housing facilities. Presence of a copulation plug in the morning was recorded as day E0.5. All experimental protocols involving mice described in this publication have been approved by the University of Minnesota Institutional Animal Care and Use Committee.

ES Cell Culture

ES cells were maintained in a 37°C 5% CO2 incubator on irradiated mouse embryonic fibroblasts (MEFs) or gelatin coated plates in Knock Out Dulbecco's Modified Eagles Medium (KO-DMEM, Invitrogen) supplemented with 15% ES cell certified fetal bovine serum (ES-FBS, Hyclone), 0.1 mM non-essential amino acids (NEAA), 2 mM L-glutamine, 0.1 mM 2-mercaptoethanol (BME), 100 U/ml penicillin, 100 μg/ml streptomycin (Invitrogen) and 1000 U/mL ESGRO (recombinant mouse LIF, Chemicon).

Generation of a conditional *Bcor* deletion targeting construct

Two independent end-sequenced 129S7/AB2.2 BAC clones (Adams et al., 2005), bMQ406j09 and bMQ339j09, were identified via Ensembl DAS Resource to contain the genomic fragment of *Bcor* necessary to generate the targeting construct. Both clones, obtained from the Sanger Institute, were verified by polymerase chain reaction (PCR) to contain the correct genomic fragment. The *Bcor* genomic fragment spanning the entire length of both homologous arms was retrieved into pBluescript based vector PL253 from isolated BAC DNA and *loxP* sites, *frt* sites, and the Pgk-Neo selection cassette were introduced by recombineering as described (Liu et al., 2003). Recombineering reagents including vectors and bacterial strains were supplied by the Copeland/Jenkins lab. Recombineering primers as defined by (Liu et al., 2003) are listed below:

Recombineering A: 5'-ATGAGCTGCGGCCGCAGGTTTCTAAGGGTTTGAAGAATGG-3'

Recombineering B: 5'-ATACTAGTTGCCTCAGTTCCTTACATGACAAG-3'

Recombineering C: 5'-GATGTCGACGTATGCAGAGACCACCTCTTGGC-3'

Recombineering D: 5'-AGAATTCGTTCGTTGGCAAGGTTGTGG-3'

Recombineering E: 5'-TGGATCCTCCCGCTGCCTCAGTCATCA-3'

Recombineering F: 5'-GATCTGCCGCGGTGATCACTGGAGCGGCTTCA-3'

Recombineering G: 5'-ACGGTACCGTCAGGGTAGAAAAACCAAAGCAAG-3'

Recombineering H: 5'-ACGGGCCCAGCATAAGCCACCCTAAATAGAGCT-3'

Recombineering I: 5'-AGGATCCATTGCTGGTAGAAAGGTGGTCTTG-3'

Recombineering J: 5’-CATCAGCCGCGGTGTGGATCATGCAGGCTTGG-3’

Recombineering Y: 5’-TGACTAGTGAAGTGAACTGAACAGGTTTTCCTG-3’

Recombineering Z: 5’-TGGATCCGCCTGGTGTACAGAGTGATTCTAGG-3’

Generation of *Bcor* ^{Neo2} ES cells

The final *Not1* linearized targeting vector was electroporated into 129S1 CJ7 ES cells, and DNA was isolated from 96 G418 resistant ES cell clones, *Apa1* digested, and screened by Southern blot hybridization with a DNA probe specific for sequence immediately flanking the 5’ arm of the targeting vector. Five homologous recombinants were identified and homologous recombination was reconfirmed by Southern blot hybridization using a DNA probe for sequence immediately flanking the 3’ arm. Primers for probe generation:

5’ Bcor Southern F: 5’-GGCTGCCACAGTGATGAAGTTG-3’

5’ Bcor Southern R: 5’-CCTTTCTCCAAGCCTCTTAGGG-3’

3’ Bcor Southern F: 5’-TCCTGAGTGTCCTGGTTTCCTAATA-3’

3’ Bcor Southern R: 5’-TGCCCGAAACCATACTGTGCA-3’

Generation of *Bcor* $^{\Delta E9-10/Y}$ ES cells by *in vitro* Cre recombination

Bcor ^{Neo2} ES cells were passaged onto irradiated MEFs and immediately infected with 5 uL of an Adenovirus (Ad5ΔE1ΔE3) (5X10^4 pfu/uL) expressing an EF1-alpha promoter driven codon-optimized EGFPCRE fusion protein. This adenovirus was created by recombination of pBS598 (Le et al., 1999) (Addgene plasmid 11923). Forty-eight hours later, cells were treated with trypsin, filtered to ensure single cell suspension, and ES cells expressing high levels of EGFP were single cell sorted into 96 well plates containing irradiated MEFs and new ES cell media. Individual cells were expanded and screened for successful Cre-mediated recombination via PCR and western blot analysis.

Generation of a transgenic conditional Bcor expression Rosa26 targeting construct—The conditional myc-tagged *BcorA* targeting vector for the *Rosa26* locus was generated in three steps. First, a single myc-tag was added to the 5’ end of mouse *Bcor* splice version A cDNA by PCR. Second, this 5’ myc-tagged *Bcor* fragment and the remaining 3’ *Bcor* coding sequences were inserted into the multiple cloning site of pBigT (Srinivas et al., 2001). Third, the resulting conditional cassette was excised and inserted into pROSA26-PA (a gift of Frank Costantini (Addgene plasmid # 21271; http://n2t.net/addgene:21271; RRID:Addgene_21271) (Srinivas et al., 2001), to flank the conditional cassette with 5` and 3` Rosa26 homology arms of 1.1 and 4.3 kb, respectively.

Generation of *Rosa26*^{LsLmBcorA} ES cells

The final *KpnI* linearized Rosa26 targeting vector was electroporated into 129S1 CJ7 ES cells and DNA was isolated from 384 G418 resistant ES cell clones, *EcoRV* digested, and

screened by Southern blot hybridization with DNA probes designed to detect both wild type (11.5 kb) and targeted (4.1 kb 5' and 16.5 kb 3') alleles. Primer sequences are as follows:

5' Rosa Southern F: 5` – AATACCCAGGCAAAAAGGGGAGACC – 3`

5' Rosa Southern R: 5` – GCTCAGAGACTCACGCAGCCCTAGT – 3`

3' Rosa Southern F: 5` – CTGTCTGAGCAGCAACAGGTCTTCG– 3`

3' Rosa Southern R: 5` – CACAATATTGCTCGCACCAACACAA– 3`

Generation of mice with conditional *Bcor* alleles

Homologously targeted and karyotypically normal *Bcor* $^{Neo2/Y}$ and *Rosa26* ^{LsLmBcorA} ES cells were separately injected into C57BL/6 blastocysts by the University of Minnesota Mouse Genetics Laboratory to generate chimeras. Chimeric mice displaying high contribution from ES cells were mated to wild type C57BL/6 mice, and female offspring were screened for germline transmission of the targeted allele via coat color and genotyping. *Bcor* $^{+/Neo2}$ mice were further mated to male β-*actin-Flpe* transgenic mice (Rodriguez et al., 2000), resulting in excision of the Pgk-Neo selection cassette and the generation of male *Bcor* $^{Fl/Y}$ and female *Bcor* $^{Fl/+}$ mice. The following mouse lines will be available from The Jackson Laboratory: BcorFL (JAX#035713) and Rosa26LsLmBcorA (JAX#035714).

Mouse breeding

All breeding, unless indicated otherwise, was done on a mixed genetic background, mainly 129S1:C57BL/6N. For generation of OFCD females, *Bcor* $^{Fl/Y}$ males were bred to *β-actin-Cre* females (Lewandoski et al., 1997) (a gift of M. Lewandoski). For all other crosses *Bcor* $^{Fl/Fl}$ females were bred to males containing one of eight *Cre* alleles. For global deletion and extraembryonic studies the *β-actin-Cre* was used. For deletion in neural crest cells we used a *Pax3* null mutation with *Cre* replacing exon 1 of *Pax3* (Lang et al., 2005) (JAX stock #005549) or a transgene with *Cre* driven by the *Wnt1* promoter/enhancer region (Danielian et al., 1998) (JAX stock #003829). For deletion in hindlimb mesenchyme progenitor cells and second heart field cells we used an *Isl1* knock-in *Cre* allele (Yang et al., 2006) (gift of S. Evans). For deletion in myocardial cells throughout the heart tube from the onset of cardiac commitment, but not in cells of the outflow tract, we used a transgenic *Nkx2.5-Cre* allele (McFadden et al., 2005) (gift of E. Olson). For deletion in both myocardial and endocardial cells, and in both primary and second heart fields, we used an *Nkx2.5-IRES-Cre* knock-in allele (Stanley et al., 2002) (a gift of R. Harvey). For deletion in cardiomyocytes, including those in the proximal but to a lesser extent the distal outflow tract, we used an *xMlc2-Cre* transgene (Breckenridge et al., 2007) (a gift of T. Mohun). For deletion in the epiblast derived tissue but not the trophectoderm, *Sox2-Cre* was used ((Hayashi et al., 2002), JAX stock #004783). The resulting *Bcor* $^{Fl/+}$ heterozygotes and *Bcor* $^{Fl/Y}$ hemizygotes served as controls, and *Bcor* $^{Fl/Y}$ mice containing the *Cre* allele were used as experimentals. For visualizing mesodermal cells *Flk1-LacZ,* mice were used (Ema et al., 2006) (a gift of J. Rossant). For *Pgk-Neo* cassette removal, *Flpe* mice were used (Rodriguez et al., 2000) (a gift of S. Dymecki).

Genotyping of *Bcor*, *Bcor* ^{Fl} and *Bcor* $^{\Delta E9-10}$ alleles

A multiplexing PCR strategy was used to genotype wild type *Bcor*, *Bcor* ^{Fl}, *Bcor* $^{\Delta E9-10}$ and *Cre* alleles from genomic DNA isolated from mouse tails and embryonic yolk sacs. Primers C or C2 and G at 0.2 μM each, and J at 0.4 μM generate a wild type amplicon of 424 bp, a *Bcor* ^{Fl} amplicon of 570 bp, and a *Bcor* $^{\Delta E9-10}$ amplicon of 519 bp with primer C or 510 bp with primer C2 (Fig. 1B, E), while Cre primers at 0.2 μM each generate an amplicon of 372 bp using the following conditions: 94°C, 4min, then 36 cycles of the next three amplification steps 94°C, 30sec, 60°C, 30 second, 72°C, 1 min., then 72°C, 10 min. All five primers can be run together and resolved on a 1.5% agarose gel (not shown).

Bcor C: 5'-GATGTCGACGTATGCAGAGACCACCTCTTGGC-3'

Bcor C2: 5'-GTATGCAGAGACCACCTCTTGGC-3' (without SalI restriction site)

Bcor G: 5'-ACGGTACCGTCAGGGTAGAAAAACCAAAGCAAG-3'

Bcor J: 5'-CATCAGCCGCGGTGTGGATCATGCAGGCTTGG-3'

Cre forward: 5'-CCTGATGGACATGTTCAGGGATCA-3'

Cre reverse: 5'-TCCATGACTGAACGAACCTGGTCG-3'

In the cases where genotyping of embryos needed to be done from tissue scraped from slides (i.e whole decidua), H&E stains were performed to identify the embryonic tissue to be scraped. An adjacent slide was stained with only Nuclear Fast Red (VWR Amresco #1B1369), rinsed in tap water and allowed to dry. A small puddle of water was pipetted onto the area to be scraped, the desired tissue was scraped with the tip of a scalpel blade and the fragments were transferred to a 1.5 mL microfuge tube with a pipettor. The tissue was pelleted for 2 min at top speed and the water was removed. Then 50 uL of TENS/PK + 200mM NaCl (50mM Tris pH8.0, 20mM NaCl, 1mM EDTA, 1% SDS, 200ug/mL Proteinase K plus an additional 200mM NaCl) was added to the pellet and incubated at 55°C overnight. The next day, 16.5 uL of saturated NaCl was added, mixed and incubated at −20°C for 10 min., spun at top speed for 10 min. and the supernatant was transferred to a fresh tube. An equal amount to 2-propanol was added, mixed and incubated at −20°C for 10 min. The samples were spun at top speed for 10 min, the supernatant was removed and the pellet was washed with 1 volume of 70% ethanol. After spinning the sample at top speed for 10 min., the supernatant was removed and the pellet was allowed to air dry. The pellet was resuspended in 20 uL of 1XTE (10mM Tris pH8.0, 1mM EDTA and 1–2 uL was used for PCR genotyping, as above.

Genotyping of *Rosa26* alleles

Two different PCRs on DNA prepared from mouse tails or embryonic yolk sacs were carried out. The wild type *Rosa26* allele was identified using the following primers, which generate an 800 base pair product:

Rosa26 F: 5'- GCTCTCCCAAAGTCGCTCTGAG -3'

Rosa26 R: 5’- GCCCCAGCTACAGCCTCGATTTGTG-3’

The *Rosa26* insertion allele was identified using the following primers, which generate a 320 base pair product:

Rosa26 F: 5’- GCTCTCCCAAAGTCGCTCTGAG -3’

Rosa26 Insert R: 5’- AAGACCGCGAAGAGTTTGTC-3’

Tissue processing

Tissues were immersion-fixed in 4% paraformaldehyde fixative (Electron Microscopy Sciences) overnight at 4 degrees Celsius or in 10% buffered formalin (Fisher) overnight at room temperature. Following fixation, tissues were ethanol dehydrated, cleared in CitriSolv (Fisher) or Xylenes, and infiltrated with Paraplast Xtra paraffin wax (McCormick Scientific) at 60 °C and 20 psi or infiltrated using a Leica TP1020 tissue processor. Following infiltration, tissues were embedded and cut into 5–7 micron sections using a Leica or Microtom rotary microtome.

In-situ hybridization

In situ hybridization analysis was performed as previously described (Wamstad and Bardwell, 2007). Briefly, the digoxigenin-labeled antisense and sense riboprobes were synthesized by *in vitro* transcription using the MEGAscript T7/T3 kit (Ambion, Austin, TX). Previously described plasmids used for riboprobe synthesis were *Bcor* exon 4 (Wamstad and Bardwell, 2007), *Uncx4.1*, *Fgf8* (Hamasaki et al., 2004), *Foxg1* (Nakagawa and O’Leary, 2003), and *Otx2* (Ang et al., 1994). The *Bcor* exon 9–10 in situ probe plasmid construct was made by PCR amplifying nucleotides 3906 to 4410 from mouse *BcorA* cDNA (pcDNA3.1.mBCoRA gift from C. Hemenway) using primers:

BcorE9–10 F: 5’-CAATGCAAGTGGCAAAAAGCAG-3’

BcorE9–10 R: 5’-GAGGGTCTCGCCAGCATTCTTA-3’

The PCR product was then cloned into pCR 2.1TOPO vector using a TOPO TA kit (ThermoFisher) and then subcloned into pBluescript KS vector using restriction sites *KpnI* and *XbaI*. *Bcor* 9–10 antisense probe was generated by PCR using the following primers and transcribing with T7 polymerase:

BcorE9–10 F: 5’-CAATGCAAGTGGCAAAAAGCAG-3’

T7: 5’-AATACGACTCACTATAGGG-3’

Lectin staining

Lectin staining was performed as described (Hemberger et al., 1999) with some modifications. Placentas were harvested and fixed in 4% paraformaldehyde overnight at room temp and processed for routine paraffin embedding. Sections were cut at a thickness of 7um, deparaffinized and boiled in 10mM sodium citrate acid buffer pH6.0 for 15 min for antigen retrieval. Sections were treated with 3% H_2O_2, incubated with peroxidase-

conjugated lectin BS-I B4 (Sigma, L5391), stained using the Liquid DAB and Substrate Chromogen System (Vector Labs, SK4100) and counterstained with Gill's Hematoxylin (Sigma).

LacZ staining

LacZ staining was performed as described (Anderson et al., 2004) with modification as in the protocol at http://www.cvri.ucsf.edu/~bblack/wp-content/uploads/2012/04/X-gal_staining_embryos.pdf

Tissue and skeletal staining and skeletal preparations

Mutant and control sections were dewaxed and rehydrated in a decreasing ethanol series. Rehydrated tissue was stained with Harris Hematoxylin (Sigma), acid washed, treated with bluing reagent and Eosin Y (Sigma) stained. Stained sections were dehydrated and mounted using Permount mounting medium (Fisher). Images were captured with Axiovision (release 4.6) software (Zeiss). Captured images were then further processed using Adobe Photoshop CS3. Digital manipulation was used to adjust color balance for some H&E and skeletal images and where done was applied equally to the whole image and to both controls and experimental samples. Trichrome staining was as described (Vialli, 1951). Bone and cartilage staining was carried out as described (Depew, 2008). For skeletal preparations animals were euthanized, skin and internal organs removed, and the carcasses subjected to dermestid beetle cleaning (Hefti et al., 1980).

qRT-PCR primers

Bcor exons 1 to 3 primers (endogenous)

Forward: 5'- CAGGGCTCCCTGCCTACTTC -3'

Reverse: 5'- GAAGCGTCGCCATCATTCAC -3'

Bcor exons 8 to 9 primers (works on human and mouse)

Forward: 5'- GGCAAAGCAGGAAGGAAGTG -3'

Reverse: 5'- CTTGGCTGAGCCTGCTTTTT -3'

Cdkn2a locus

Forward: 5'- GGACCAGGTGATGATGATG -3'

Reverse: 5'- ATCGCACGATGTCTTGATG -3'

Hprt

Forward: 5'-AGCTACTGTAATGATCAGTCAACG-3'

Reverse: 5'-AGAGGTCCTTTTCACCAGCA-3'

Palatal shelf cultures

The palatal shelf culture protocol was a modified version of those previously described (Abbott, 2003; Jaskoll et al., 2003). Embryos were harvested from pregnant mice at E12.5, and palatal shelves were dissected into Hanks Balanced Salt Solution supplemented with 2.38 mg HEPES per ml and 50 units penicillin/streptomycin antibiotic per ml. Explants were then placed, nasal pits oriented downwards, onto sterile 0.8 um filter paper and grown for 5 days on a stainless-steel mesh grid overlying BGJb medium (Invitrogen) supplemented with 0.1 mg vitamin C per ml and 50 units penicillin/streptomycin antibiotic per ml in a 37 °C incubator at 5% CO_2.

Eye analysis

Lens opacification was detected visually using an ophthalmoscope. Dissected eye globes were fixed in 10% buffered formalin (Fisher) overnight and stored in 70% ethanol. Globe width was measured with high precision calipers.

Western Blot Analysis

ES cells were incubated in lysis buffer (1X phosphate buffered saline (PBS), 10% glycerol, 0.5% Nonidet-P40, 2 mM dithiothreitol (DTT), 0.2 mM phenylmethylsulphonylfluoride (PMSF) and 1X Complete Protease Inhibitor (Roche)), sonicated, normalized by Bradford Assay, and resolved on a NuPAGE 3–8% Tris-Acetate gel (Invitrogen). Proteins were transferred overnight at 4°C to a nitrocellulose membrane, blocked with non-fat dry milk, and incubated with affinity purified polyclonal anti-BCOR (RRID:AB_2716801, (Gearhart et al., 2006)) and monoclonal anti-β-ACTIN antibodies (SC-47778 Santa Cruz). ES cell westerns were visualized with ECL Blotting Reagents (GE Healthcare, #RPN2109). Mouse E9.5 embryos and placentas were harvested and put into Trizol Reagent (Ambion, ThermoFisher). Protein was isolated according to the manufacturer and resolved on a NuPAGE 3–8% Tris-Acetate gel (Invitrogen). Proteins were transferred overnight at 4°C to a nitrocellulose membrane, then blocked with 0.1% casein, 0.2x PBS and incubated with affinity purified polyclonal anti-BCOR (RRID:AB_2716801, (Gearhart et al., 2006)) and 9E10 anti-myc (Santa Cruz sc-40) or anti-β-ACTIN (47778 Santa Cruz) antibodies in 0.1% casein, 0.2x PBS, 0.1% Tween. Secondary antibodies goat anti-mouse IgG-Alexa 680 and goat anti-rabbit IgG-Alexa790 (Jackson ImmunoResearch). After washes in 1x PBS, 0.1% Tween and 1x PBS, the blot was analyzed using a LI-COR Odyssey infrared imaging system.

Results

Generation of a conditional *Bcor* deletion allele and *Bcor* $^{\Delta E9-10/Y}$ ES cells

BCOR is an essential gene in humans (Ng et al., 2004). Therefore, to bypass early lethality and investigate the role of *Bcor* in mouse development, we generated a conditional *Bcor* allele. Because *Bcor* is a large and complex gene and a previous mutant deleting exon 3 failed to eliminate function due to use of a downstream start codon (Wamstad et al., 2008), design of this conditional allele was guided by more recent clinical and molecular data. The common feature of human OFCD *BCOR* mutations, whether they are complete

gene deletions or frame shifts scattered across the length of the gene, is that the region encoding part or all of the PCGF1/3/KDM2B interacting region (exons 10–15, (Gearhart et al., 2006; Junco et al., 2013; Wang et al., 2018) is deleted. For example, in-frame deletion of human exon 10, as a consequence of a splice site mutation, results in the full clinical presentation of OFCD, indicating that exon 10 is required for *BCOR* function (Fig. 1A, see legend note) (Ng et al., 2004). Additionally, mutations in exon 9 of *BCOR* that result in a premature stop codon have been found in multiple OFCD patients (Hilton et al., 2009; Ng et al., 2004). Based on these data, removal of exons 9 and 10 (which are orthologous in the mouse) should allow splicing of exon 8 to 11, but generate an mRNA with a premature stop codon, eleven amino acids after the resulting splice junction. This deletion would closely recapitulate OFCD mutations in humans. If the premature stop codon does not trigger nonsense-mediated mRNA decay, any truncated protein produced would be unable to associate with critical PRC1.1 complex components. Thus, we predict the resulting conditional allele should exhibit severe loss-of-function after CRE-mediated recombination. However, we cannot formally rule out the possibility that the residual levels of the truncated protein, should they exist, may retain functions independent of the interactions with Polycomb proteins. Fig. 1 B and C illustrates this conditional targeting strategy and successful homologous recombination in ES cells.

To determine the effect of Cre-mediated exon 9–10 deletion on *Bcor* transcript levels and protein production, we generated an ES cell line with the deleted allele ($Bcor^{\Delta E9-10}$). We treated $Bcor^{Neo2/Y}$ ES cells with adenovirus-expressing CRE recombinase and screened for successful deletion by PCR. In the mutant ES cells RT-PCR analysis using primers from outside the deleted region showed that *Bcor* mRNA levels were reduced by 40%, suggesting that the resulting premature stop codon caused some non-sense mediated decay. Western blot analysis of ES cell protein extracts (Fig. 1D) revealed that targeted ES cells containing the *Neo* cassette ($Bcor^{Neo2/Y}$) express BCOR protein at a normal level compared to wild type ES cells ($Bcor^{+/Y}$). After deletion of exons 9 and 10 ($Bcor^{\Delta E9-10/Y}$), wild type BCOR protein was absent, and a C-terminally truncated form of BCOR of the expected size lacking the PCFG1/3 and KDM2B interfaces, designated BCORΔE9–10, was present. The truncated BCORΔE9–10 product in targeted and deleted ES cells was present at a significantly reduced level compared to full length BCOR in $Bcor^{+/Y}$ non-targeted or $Bcor^{Neo2/Y}$ non-deleted ES cells. The $Bcor^{\Delta E9-10/Y}$ cells maintained ES cell morphology throughout multiple passages and had a similar doubling time to $Bcor^{+/Y}$ and $Bcor^{Neo2/Y}$ cells when grown on mouse embryonic fibroblasts (MEFs) in the presence of LIF. $Bcor^{\Delta E9-10/Y}$ cells also maintained ES cell morphology in a defined culture system (plated on gelatin in the presence of LIF) although with a slightly reduced doubling time relative to wild type ES cells (data not shown). Thus, *Bcor* is not required for ES cell self-renewal under these conditions. In contrast, the combined loss of RING1 and RNF2, the enzymatic core of all PRC1 complexes, results in loss of ESC self-renewal (Endoh et al., 2008) suggesting that *Bcor* and, thus PRC1.1, plays its first essential role later role in development, as indicated by our previously generated hypomorphic $Bcor^{Neo}$ allele (Wamstad et al., 2008).

Next, we generated mice with the $Bcor^{Fl}$ allele. Chimeric mice were created by blastocyst injection of targeted ES cells ($Bcor^{Neo2/Y}$), and germline transmission gave rise to female $Bcor^{+/Neo2}$ progeny, carrying the targeted allele with the neomycin selection cassette still in

place. In contrast to our previous *Bcor* ^{Neo} allele with exon 3 flanked by *loxP* sites (Wamstad et al., 2008), no physical abnormalities or variations in coat color contribution bias were observed in chimeric male *Bcor* $^{Neo2/Y}$ or female *Bcor* $^{+/Neo2}$ mice, suggesting normal expression of *Bcor* from this new *Bcor* ^{Neo2} allele. We used *in vivo* FLPe recombination (Rodriguez et al., 2000) to remove the *Neo* cassette and generate mice harboring the floxed allele of *Bcor* (*Bcor* ^{Fl}) (Fig. 1 B, E). *Bcor* $^{Fl/Fl}$ and *Bcor* $^{Fl/Y}$ animals were bred to maintain the allele. These mice had normal litter sizes and life span and no observable phenotypes, indicating the *loxP* sites were not disruptive to normal expression and splicing. Thus, we were able to use this *Bcor* ^{Fl} allele to examine the effect of: i. heterozygous *Bcor* mutation in females, (*Bcor* $^{+/\Delta E9-10}$, modeling OFCD); ii. *Bcor* mutation in males (*Bcor* $^{\Delta E9-10/Y}$); and iii. *Bcor* conditional deletion in specific embryonic cell types and the extraembryonic compartment.

Bcor heterozygosity in females reduces postnatal viability

To model OFCD, we generated heterozygous *Bcor* $^{+/\Delta E9-10}$ females by breeding females carrying the ubiquitous *Cre* transgene *β-actin-Cre* (Lewandoski et al., 1997) *to Bcor* $^{Fl/Y}$ males (Fig. 1F, left). This cross generates experimental female *Bcor* $^{+/\Delta E9-10\ (p)}$ ("*OFCD animals*"; genotype *Bcor* $^{+/Fl}$:*β-actin-Cre*, with the mutant *Bcor* allele randomly X-inactivated in the embryo but paternally silenced (p) in the extraembryonic tissue, see below) and controls (genotypes *Bcor* $^{+/Fl(p)}$, *Bcor* $^{+/Y}$:*β-actin-Cre,* and *Bcor* $^{+/Y}$). To determine whether there was any embryonic lethality of OFCD animals we dissected out and genotyped 55 late gestation embryos (E17.5 and later). The genotypes did not deviate from the expected Mendelian ratios (Chi-square = 1.76, p = 0.41) indicating there was no loss of viability for prenatal OFCD animals. Next, we examined the genotypes of 373 animals that survived to weaning from 54 litters. Among these were 225 males (all wild type for *Bcor* $^{+/Y}$, either with or without *β-actin-Cre*), 98 *Bcor* $^{+/Fl}$ females and 50 OFCD females. This is significantly different from the expected Mendelian ratio (Chi-square = 28.25, p = <0.00001) and indicates that postnatal OFCD female viability is reduced to about 50%. We recorded 42 deaths between P0.5 and weaning, likely accounting for many of the "missing" OFCD females. These data suggest that the majority of OFCD death does not occur in the very early (P0 to P0.5) postnatal period but rather between P0.5 and weaning.

Since OFCD patients are reported to have palatal clefting (24%) or high arched palate (5%) (Hilton et al., 2008; Hilton et al., 2009; O'Byrne et al., 2017; Ragge et al., 2018) and cleft palate is a common cause of death in the postnatal period in mice (Kaartinen et al., 1995; Turgeon and Meloche, 2009), we examined pups dissected from late gestation litters (E14.5 - E21.5). Clefting was observed in 32% (7/22) of OFCD females but not in the 55 male and female littermate controls (Fig. 1G). Thus, palatal clefting is likely a cause of postnatal death in OFCD animals. Cardiac defects, which are observed in OFCD patients (Hilton et al., 2008; Hilton et al., 2009; O'Byrne et al., 2017; Ragge et al., 2018), may also contribute to postnatal death (see below). The surviving OFCD animals always have kinky tails (Fig. 1 H) and tend to be slightly smaller than their littermates during the pre-weaning and early post-weaning period (Fig. 1I), but as adults they are similar in size to controls (not shown).

We backcrossed *β-actin-Cre* and the *Bcor* ^{Fl} allele to the C57BL/6N background and bred to generate OFCD animals and controls. At E18.5 the genotypes did not deviate from the expected Mendelian ratios (Chi-square = 0.44, p = 0.80) and similar to the mixed background 33% of fetuses had cleft palates. We then examined the genotypes of 230 animals from 37 litters that survived to weaning. Among these were 151 males (all wild type for *Bcor*), 75 *Bcor* $^{+/Fl}$ females but only 4 OFCD females. This significant deviation from the expected Mendelian ratio (Chi-square 66.37, p = <0.00001) indicates that postnatal OFCD female viability is further reduced on the C57BL/6N background to about 5%. We recorded only 11 deaths between P0.5 and weaning, likely accounting for only about 15% of the "missing" OFCD females. We presume the remaining missing OFCD females died in the immediate (P0-P0.5) postnatal period. We have not investigated the causes of the increased severity of the phenotypes on the C57BL/6N background further here but focused on analysis the OFCD mice that survive on the mixed background as they are a model for the surviving OFCD patients.

Bcor heterozygosity in females causes OFCD-like defects

We next asked whether the surviving OFCD mice on the mixed background have developmental phenotypes similar to those of human OFCD patients. Importantly, female OFCD patients express their mutant *BCOR* allele in a mosaic manner due to random X chromosome inactivation (XCI) during early embryogenesis, and as a result their OFCD-associated phenotypes are expressed to variable degrees (Hilton et al., 2009). This variable expressivity should occur in OFCD mice since mice also undergo random early XCI in inner cell mass-derived cells of the blastocyst (Lyon, 1961). In addition, XCI occurs with different timing in different somatic tissues (Tan et al., 1993). As a result, some tissues may progress further in development with two active X chromosomes before random XCI. Thus, some tissues may not be affected if a critical window of *Bcor* activity has been by passed. As described in the following paragraphs, we find that *Bcor* heterozygous mice do manifest many of the most common phenotypes seen in the human OFCD syndrome with variable expressivity consistent with mosaic expression of the mutant X chromosome.

Essentially all described OFCD patients have congenital cataracts, usually bilateral, and 64% have microphthalmia, often more pronounced in one eye (Hilton et al., 2008; Ragge et al., 2018). OFCD and littermate control mice (ranging from 3 to 28 weeks), were examined for lens opacification, which is indicative of cataracts. Fifty-five percent (23/42) of OFCD animals had lens opacification, and in these animals 8/23 were affected bilaterally while none of the 28 control animals had lens opacification (Fig. 2A). Since 75% of the younger (3–6 week) animals had cataracts, these are most likely congenital, as in humans. Next, we sacrificed a cohort of adult animals (7 controls and 15 OFCD), dissected out the eye globes, and measured their widths. On average the width of all OFCD globes was 0.2 mm less than that of controls (Fig. 2B). In addition, there was pronounced bilateral asymmetry of the globe width in the OFCD animals; the median difference between wider and narrower globe width was 4.5-fold greater in OFCD animals vs. controls (Fig. 2C). A one-year old OFCD mouse with pronounced microphthalmia in the left eye is shown relative to a littermate control (Fig. 2 D, E).

As described earlier, OFCD patients tend to have a distinctive set of facial and cranial features. We did not carry out a quantitative assessment of craniofacial dysmorphogenesis due to the variable expressivity of phenotypes, but OFCD mice snouts were occasionally broader or asymmetric, as in Fig. 1I, middle and Fig. 2 E, F. *Bcor* is expressed in the eyelid progenitor cells (Wamstad and Bardwell, 2007) and often the eyelids of OFCD animals appeared ptotic and/or swollen and more prone to closure, which, together with the microphthalmia, was the most common recognizable facial feature (Fig. 2 E, F).

Skeletal abnormalities in OFCD patients include scoliosis and other vertebral skeletal defects such as vertebral fusions, hammer toes, and second-third toe syndactyly. OFCD mice often develop kyphosis, which was most obvious in older animals. To further investigate curvature of the spine we used dermestid beetles to generate skeletal preparations of 9 control and 16 OFCD animals. Kyphosis but not scoliosis was observed (Fig. 2G). We measured the kyphosis index (KI) (Laws and Hoey, 2004) of the control and OFCD adult mice (8.5 – 13 months), and found that OFCD animals have a lower KI relative to controls, indicative of kyphosis (Fig. 2H). No obvious wedging of the vertebral discs was observed, suggesting the kyphosis may be due to an age-related cartilage or musculature defect rather than skeletal defects. We did not observe syndactyly or hammer toes in any of the skeletal preparations of OFCD or control animals.

OFCD patients can have cardiac abnormalities, most commonly septal defects, as well as dental abnormalities such as delayed dentition, extended tooth growth, extra teeth, and fused teeth. We used echocardiography to assess cardiac function in three adult OFCD mice and did not observe obvious cardiac defects, although those with severe defects may have already died before weaning. The OFCD mice occasionally manifested dental abnormalities (VJB, PTS, unpublished data). Laterality defects have been noted in some OFCD patients (Hilton et al., 2007). We examined intestinal and heart polarity in 15 OFCD mice but did not observe obvious polarity reversal. In summary, OFCD mice exhibit cleft palate, a likely cause of reduced postnatal survival, cataracts, microphthalmia, ptosis, and kyphosis, all with variable penetrance, similar to OFCD patients.

Mutation of *Bcor* in males results in early embryonic lethality

Male OFCD patients have never been reported, indicating that mutation of *BCOR* likely results in embryonic lethality. Indeed, in a screen of aggregation chimeras from XY ES cells with X-linked gene traps, *Bcor* loss of function resulted in early lethality in the mouse (Cox et al., 2010). To examine in more detail the effects of *Bcor* loss-of-function on early development, we bred $Bcor^{Fl/Fl}$ female mice to males carrying the *β-actin-Cre* transgene (Fig. 1F, right). This cross generated experimental $Bcor^{Fl/Y}$:*β-actin-Cre*, ($Bcor^{\Delta E9-10/Y}$) animals deleted at or before the blastocyst stage, as well as control $Bcor^{Fl/Y}$ and $Bcor^{Fl/+}$ animals. (Analysis of $Bcor^{Fl/+}$;*β-actin-Cre* concepti ($Bcor^{\Delta E9-10/+(p)}$) from this cross is described in a later section on extraembryonic development.)

We first examined *Bcor* expression by *in situ* hybridization in concepti from this $Bcor^{Fl/Fl}$ to *β-actin-Cre* cross at E7.5 and E8.5 using a *Bcor* probe spanning exons 9 and 10 that detects wild type *Bcor* mRNA but not *Bcor* mRNA from the deleted allele. As previously reported *Bcor* normally is highly expressed in extraembryonic tissues and more weakly in

the developing embryo (Fig. 3 A, C, E, G, I, K) (Wamstad and Bardwell, 2007). In *Bcor* $^{\Delta E9-10/Y}$ concepti, which are visibly smaller, this hybridization was lost indicating that CRE excision was efficient (Fig. 3 A and E vs. B and F). To determine whether *Bcor* mRNA from the exon 9–10 deleted allele harboring a premature stop codon was targeted for nonsense mediated decay, we used an exon 4 probe that detects all *Bcor* transcripts at E8.5. *Bcor* RNA was detected in *Bcor* $^{\Delta E9-10/Y}$ and *Bcor* $^{\Delta E9-10/+(p)}$ embryos at levels approximating those in control embryos (Fig. 3 I and K vs. J and L). Quantitative RT-PCR with primers spanning exons 8 and 9 on RNA from E8.5 embryos showed that the non-deleted transcript, retaining exons 9–10, is present in *Bcor* $^{\Delta E9-10/Y}$ embryos at 1% (p=0.0062, one-sided *t* test) of control levels indicating CRE deletion was very efficient. In contrast, using primers spanning exons 1 and 3, *Bcor* mRNA was found in *Bcor* $^{\Delta E9-10/Y}$ embryos at 43% (p=0.054 one-sided *t* test) of control levels relative to *Hprt*. We conclude that, as in ES cells, nonsense-mediated decay does not efficiently destroy all of the deleted transcript. However, as mentioned above, any truncated protein produced from this transcript should have severely reduced function, as it lacks the region required for interaction with PCGF1/3 and KDM2B.

Examination of embryos from timed matings of *Bcor* $^{Fl/Fl}$ females and *β-actin-Cre* males revealed that all *Bcor* $^{\Delta E9-10/Y}$ embryos were nonviable and being resorbed by E10.5. To better visualize the early embryos we included the *Flk1-LacZ* allele, which marks a broad spectrum of mesodermal progenitors exiting the primitive streak as well as later mesodermal cell types, including some cardiomyocytes, portions of the somites, and all extraembryonic mesoderm cells (Ema et al., 2006). At ~E7.5, the earliest stage examined, *Bcor* $^{\Delta E9-10/Y}$ embryos were already delayed in development relative to their littermate controls; while controls had prominent head folds and had formed the first somite pairs, *Bcor* $^{\Delta E9-10/Y}$ embryos had not (Fig. 3 M–P). This delay in development continued to be observed at E8.5, and based on developmental landmarks corresponded to approximately one half to one day of developmental time (Fig. 3 Q–T). Consistent with a half day delay, in 21 E8.5 litters examined the *Bcor* $^{\Delta E9-10/Y}$ embryos had on average 7.4 fewer somite pairs relative to *Bcor* $^{Fl/Y}$ controls. In these E8.5 litters *Bcor* $^{\Delta E9-10/Y}$ embryos were found at close to the expected Mendelian frequency (19% vs. 25%), but by E9.5 all *Bcor* $^{\Delta E9-10/Y}$ animals were dead (Fig. 3 V, W). In some of these E8.5 and dead E9.5 concepti the allantois had contacted the chorion, an event that normally occurs late in Theiler Stage 12 (usually ~ E8 to 8.75), when seven somite pairs have formed (Fig. 3W). *Bcor* $^{\Delta E9-10/Y}$ animals had often initiated but almost never completed embryonic turning, an event that occurs during Theiler Stage 13 when embryos have 8–12 somite pairs. We next considered the possibility that the developmental delay may in part reflect a proliferation defect due to a failure to repress the *Cdkn2a* cell cycle regulatory locus, as this was seen to partially underlie the developmental arrest seen in *Rnf2*-null embryos (Voncken et al., 2003). We found, using qPCR, that *Cdkn2a* mRNA levels were 5.5 fold higher (p=0.055 one-sided *t* test) in E8.5 *Bcor* $^{\Delta E9-10/Y}$ embryos vs. controls. In summary, *Bcor* $^{\Delta E9-10/Y}$ had significant delays in landmarks of embryonic development starting before E7.5, had increased *Cdkn2a* mRNA and died at or before the end of Theiler stage 13 (E9.25). Assuming death of male *BCOR* $^{-/Y}$ concepti occurs at a similar stage in humans, ~ 21 days post fertilization, it is likely that these pregnancies may not even be detected and may manifest as a late, heavy menstruation.

To look for specific defects in development of *Bcor* $^{\Delta E9-10/Y}$ vs control animals, we matched embryos by somite number rather than gestational age to attempt to control for the differences in timing of developmental progression. To examine somites themselves, we used an *Uncx4.1 in situ* probe which marks the posterior somite compartments (Mansouri et al., 1997) and found similar hybridization patterns in 8–9 somite *Bcor* $^{\Delta E9-10/Y}$ and *Bcor* $^{Fl/Y}$ embryos (Fig. 3 X–AA). Although the more posterior regions of the somite-matched embryos showed similar developmental progression the most obvious differences were in the trunk and developing brain in the *Bcor* $^{\Delta E9-10/Y}$ embryo vs *Bcor* $^{Fl/Y}$ controls (Fig. 3 X and BB vs Y and CC). The trunk was shorter and cardiac tissue was not prominent, suggesting there is a defect in cardiac development. The brain appeared smaller and misshapen. To examine the brain in more detail we did *in situ* analysis for RNAs that mark specific regions of the developing brain. *Otx2*, which is normally expressed in the forebrain and midbrain (Ang et al., 1994), was still expressed generally in the same regional pattern at the 5 and 6 somite stages although the expression level appeared somewhat lower and the forebrain appeared smaller (Fig. 3 BB–II). By the 8–9 somite stage there was an apparent lack of *Fgf8* expression in the anterior neural ridge (Fig. 3 JJ–MM). Consistent with this reduction in *Fgf8*, expression of the downstream gene *Foxg1,* a forebrain marker (Shimamura et al., 1995; Tao and Lai, 1992) was strongly reduced in the mutant by the 12 somite stage (Fig. 3 NN–QQ). Reduced *Foxg1* has previously been associated with hypoplasia of the telencephalon (Storm et al., 2006), and this is consistent with the reduced size of the forebrain seen in the *Bcor* $^{\Delta E9-10/Y}$ embryos.

Bcor is required in embryonic neural crest lineages for postnatal survival

Next, we used conditional gene targeting to try to bypass the early embryonic lethality of *Bcor* $^{\Delta E9-10/Y}$ mutants and investigate in which cell lineages *Bcor* plays important developmental roles. *BCOR* in these lineages would also be likely to contribute to OFCD phenotypes in *BCOR* $^{-/+}$ females. We initially deleted *Bcor* exon 9–10 using *Pax3-Cre* (Lang et al., 2005), which is expressed primarily in neural crest and somite lineages, but also in scattered cells of other tissues (Engleka et al., 2005). Since *Bcor* is X-linked, the breeding scheme for this and subsequent cell type-specific *Cre* alleles involved crossing males carrying the *Cre* allele with *Bcor* $^{Fl/Fl}$ females and examining the phenotype of the hemizyous males without or with *Cre*. Conditionally targeted animals (*Bcor* $^{Fl/Y}$;*Pax3-Cre*) were found at Mendelian ratios throughout embryonic development, but no surviving mutants were observed at weaning. Mutant animals were born at normal size compared to wild type littermates but failed to thrive, exhibited a pale gray coloring, and died without milk spots within a few hours of birth (data not shown). To confirm that this lethality reflected a neural crest requirement rather than defects in somite-derived tissues or other *Pax3* expressing cells, we deleted exons 9 and 10 of *Bcor* specifically in the neural crest cell lineage using a *Wnt1-Cre* transgene that is active in pre-migratory neural crest cells (Danielian et al., 1998; Jacques-Fricke et al., 2012). Exon 9–10 deletion of *Bcor* in the *Wnt1*-expressing lineage also caused perinatal lethality with a similar failure to thrive, confirming that *Bcor* is required in the neural crest cell lineage for postnatal survival.

Bcor is required in neural crest lineages for normal palatal shelf elevation

Neural crest cells differentiate into diverse cell lineages throughout the body. Within the head, which is particularly affected in OFCD patients, they contribute to bones, cartilage, nerves and connective tissue. Given the lack of milk spots in newborn *Bcor* neural-crest-specific mutant animals, we more closely examined the mutants at E18.5 for defects that could compromise nursing. All *Bcor* mutants deleted with either *Pax3*- or *Wnt1*-Cre transgenes had severe cleft palate defects (Fig. 4 A, B and data not shown), which, as mentioned, are a common cause of death within the perinatal period (Turgeon and Meloche, 2009). Hematoxylin and eosin (H & E) staining of E18.5 frontal sections revealed that the clefting involved both the hard and soft portions of the palate (Fig. 4 C – F). Skeletal preparations of E18.5 animals further confirmed palatal clefting in the mutant animals, showing the failure of Alizarin red-stained bony structures to fuse in the palatal midline (Fig. 4 G, H). Given the timing of death in these mutants, as well as their external appearance within the perinatal period, this cleft palate defect is a likely cause of death. We conclude that *Bcor* is required in the neural crest cell lineage for appropriate formation of the palate.

To ascertain the timing and cause of the cleft palate defect, we examined mutant and wild type embryos at earlier stages of embryonic development. Frontal sections of E13.5 palates revealed normal palatal histology, with vertical palatal shelves of normal size and shape descending on either side of the tongue (Fig. 4 I, J). However, by E14.5, the tongue of mutants failed to descend within the oral cavity, and the palatal shelves failed to rise to their normal horizontal position over the tongue (Fig. 4 K, L). This phenotype persisted at E15.5, when the palatal shelves of wild type animals had met and begun to fuse in the midline (Fig. 4 M, N). BrdU incorporation assays and TUNEL staining performed at E13.5, E14.5, and E15.5 detected no difference in proliferative or apoptotic activity in mutant palatal shelves compared to those of wild type littermates (n = 2 of each genotype per time point; data not shown). These results suggest the defect in palatal shelf elevation is unrelated to cell proliferation or apoptosis within the palatal shelves. We conclude that *Bcor* functions either within the palatal shelves themselves or in the surrounding neural crest cell-derived structures (e.g. the mandible or tongue) to allow palatal shelf elevation.

Bcor mutant palates are capable of *in vitro* elevation and fusion

To determine whether the cleft palate defect observed in mutants results from a primary defect in the palatal shelves themselves or from abnormal development of the underlying structures, we used *ex vivo* palatal shelf cultures. We dissected the palatal shelves at E12.5, prior to palatal shelf elevation, and assessed subsequent elevation and fusion in culture. Four of five mutant $Bcor^{Fl/Y}$;*Pax3-Cre* palatal shelves elevated and fused at the midline by day 5, compared to six of seven $Bcor^{Fl/Y}$ controls (Fig. 4 O, P). Because mutant palatal shelves are capable of elevation and fusion in culture, we conclude that the cleft palate observed in mutant animals is secondary to defects in the formation of the mandibular region.

Bcor is required in neural crest lineages to suppress ectopic salivary gland formation

During our histological analysis of the cleft palate defect in *Bcor* mutants, we noticed that all $Bcor^{Fl/Y}$;*Wnt1-Cre;* and $Bcor^{Fl/Y}$;*Pax3-Cre* mutant animals displayed a supernumerary pair of major salivary glands (SGs) (Fig. 4D), which we examined further. In addition to the

pairs of submandibular (SM) and sublingual (SL) SGs located at the bottom of the lower jaw, an ectopic pair of SGs was found in the mutants, embedded between the tongue and the floor of the mouth, between the mylohyoid, hyoglossus, and genioglossus muscles (Fig. 5 B, E, F). Only the normal SM and SL pairs of SGs were found in the control animals (Fig. 5A). The excretory ducts of the ectopic glands opened in the same area as the excretory ducts of the SM and SL glands, at the base of the tongue. They appeared either completely independent from the SM and SL excretory ducts, or drained into the SM excretory duct shortly before this duct opened into the oral cavity (Fig. 5 C, D). In mice, the SL gland is exclusively mucous, while the SM gland is largely serous. Due to its high content in mucins, the SL gland is stained blue following trichrome staining (Fig. 5G). Although the ectopic salivary glands contained mainly serous acini, groups of mucous acini could be found on the buccal side of the gland (Fig. 5H).

Frontal sections of E15.5 and E18.5 *Bcor* $^{Fl/Y}$;*Pax3-Cre* animals revealed additional craniofacial soft tissue defects. These included ankyloglossia, which is a fusion of the tongue to the underlying mucosa, persistent elevation of the tongue, and disorganization of the tongue morphology, in addition to some instances of bifid tongue (Fig. 4 C, E, M compared to D, F, N and Fig. 5 A, C, E compared to B, D F, and data not shown). Together the ectopic salivary glands and tongue dysmorphogenesis, which may be due to the underlying ectopic salivary glands, likely change the shape of the oral cavity. It is known that the tongue, as well as the mandible, play key roles in palatal development by defining the shape of the oral cavity and thus allowing palatal shelf fusion (Barrow and Capecchi, 1999; Diewert, 1981; Huang et al., 2008; Lavrin et al., 2001; Yu and Ornitz, 2011). Therefore, the ectopic salivary glands, tongue dysmorphogenesis and/or ankyloglossia in *Bcor* $^{Fl/Y}$;*Pax3-Cre* animals may in turn affect palatal shelf elevation and fusion.

Bcor is required in neural crest lineages for normal tympanic ring bone and mandible patterning

Skeletal preparations of E18.5 animals also revealed defects in craniofacial bone structures of *Bcor* $^{Fl/Y}$;*Pax3-Cre* animals. The mutant tympanic ring bone appeared truncated and thicker and the mandible appeared shortened and smaller overall compared to the wild type structures (Fig. 5 I, K, M vs. J, L, N). We measured E18.5 left and right mandible lengths of four mutants and four controls, and found that mutant mandibles were on average significantly shorter than controls (5.27 mm vs. 5.75 mm, one-sided *t* test, p=1.6×10^−7). Meckel's cartilage is a structure that arises from the neural crest cell contribution within the mandibular prominence mesoderm and forms a template for mandibular ossification (Chai et al., 2000; Frommer and Margolies, 1971). Through its key role in patterning the mandibular region, Meckel's cartilage permits proper tongue alignment within the oral cavity and thus allows for proper palatal shelf elevation at the appropriate time in development (Chai and Maxson, 2006). Given the defects in palatal shelf elevation and mandible morphology in *Bcor* mutants, we next analyzed Meckel's cartilage formation. Alcian blue staining of embryos at E14.5 highlights the developing cartilaginous structures. By this time point, Meckel's cartilage in control embryos had an elongated shape and formed an apex at the midline of the developing mandible (Fig. 5 O, Q). However, Meckel's cartilage from mutant animals failed to properly elongate and had a broadened, curved shape in the developing

mandibular region (Fig. 5 P, R). We conclude that the mandibular defects observed in E18.5 *Bcor* mutants derive from an earlier defect in Meckel's cartilage formation. Furthermore, since similar Meckel's cartilage defects have been previously implicated in failed palatal shelf elevation (Diewert, 1981), this same defect is a likely contributing factor to cleft palate defects when *Bcor* is mutant in the neural crest cell lineage. In summary, because the palatal shelves of *Bcor* mutants can elevate and fuse in culture, it is likely that the observed palatal phenotype in mice and perhaps OFCD patients is primarily due to extra-palatal defects in the tongue, salivary gland, and/or mandible.

Bcor is required in the *Isl1*-expressing cell lineages for normal cardiac development

The OFCD cardiovascular phenotypes in humans suggest BCOR functions in one or more of the multiple cell types that contribute to the cardiovascular system. We initially used several *Cre* recombinase alleles expressed in cardiac precursor cell types to determine whether *Bcor* mutation in these cells resulted in embryonic or postnatal lethality. Mutation of *Bcor* with three *Cre* alleles did not affect survival to weaning; i. an *Nkx2.5-Cre* transgene expressed in myocardial cells throughout the heart tube from the onset of cardiac commitment, but not in cells of the outflow tract (Chi-square = 2.67, p = 0.44) (Lang et al., 2005); ii. an *Nkx2.5-IRES-Cre* knock-in allele expressed in both myocardial and endocardial cells, and in both primary and second heart fields (Chi-square = 1.14, p = 0.57) (Stanley et al., 2002); and iii. an *xMlc2-Cre* transgene expressed in cardiomyocytes and the proximal outflow tract (Chi-square = 6.5, p = 0.09) (Breckenridge et al., 2007). In contrast, no mutant animals were observed at weaning when *Bcor* was mutated with *Isl1-Cre* (Chi-square = 20.38, p = 0.0001) (Fig. 6A), which drives *Cre* expression in the second heart field (SHF). The SHF has contributions throughout the cardiovascular system, with particularly high contribution to the outflow tract, right ventricle, and vascular smooth muscle lineages (Sun et al., 2007; Yang et al., 2006). Fate mapping with a *LacZ-Cre* reporter has shown that descendants of cells expressing *Isl1-Cre* were observed uniformly in the outflow tract and right ventricle, in a majority of atrial cells and in part of the left ventricle (Sun et al., 2007; Yang et al., 2006). Given the severe consequence of the *Isl1-Cre* conditional *Bcor* mutation, we chose to perform a more detailed analysis of $Bcor^{Fl/Y}$;*Isl1-Cre* mutants. Mutant embryos were observed at close to Mendelian ratios at E13.5 but decreased there after (Fig. 6A). Gross dissection at E13.5 revealed persistent truncus arteriosus (PTA), in which the truncus arteriosus (the outflow tract) fails to properly divide into the pulmonary trunk and aorta in 65% of mutant hearts, indicating penetrance is high but not complete (Fig. 6 B–F). An additional 13% of hearts displayed aortic arch abnormalities such as interruption of the aortic arch or right-sided aortic arch (Fig. 6B). Histological analysis of mutant hearts at E13.5 and E14.5 confirmed PTA and with a perimembranous ventricular septal defect (VSD; Fig. 6 G–L and data not shown). At E18.5 two of the three surviving $Bcor^{Fl/Y}$;*Isl1-Cre* mutant animals we recovered had PTA. PTA was also found in 7% of the $Bcor^{Fl/+}$;*Isl1-Cre* embryos at E13.5 (Fig. 6B) and by weaning only 44% of the expected $Bcor^{Fl/+}$;*Isl1-Cre* animals survived (Fig. 6A). Since neural crest cells are important for outflow tract development and a proportion of neural crest cells of the outflow tract are targeted by *Isl1-Cre* (Engleka et al., 2012; Sun et al., 2007), we examined $Bcor^{Fl/Y}$;*Pax3-Cre* animals at E18.5 but failed to find PTA, indicating the PTA is not due to mutation of *Bcor* in neural crest cells (data not shown). In summary, *Bcor* plays an essential role in the *Isl1* lineage

with the majority of *Bcor* $^{Fl/Y}$;*Isl1-Cre* mutants dying between E15.5 and E16.5. This death is preceded by the appearance of PTA in many of these embryos and arch anomalies in some of these embryos. The fraction of the *Bcor* $^{Fl/+}$;*Isl1-Cre* embryos that had PTA and the reduced survival at weaning highlights how functional mosaicism due to XCI impacts the phenotype in the heterozygotes. It also suggests that prenatal and postnatal lethality due to cardiac defects may contribute to the rarity of OFCD patients surviving to diagnosis.

Bcor is required in the *Isl1*-expressing cell lineage for limb patterning

Bcor is expressed in the mouse limb buds beginning at E9.5 (Wamstad and Bardwell, 2007) and syndactyly is frequently observed in OFCD patients. To analyze the embryonic requirement for *Bcor* in hindlimb patterning, we again conditionally deleted *Bcor* using the *Isl1-Cre* knock-in allele, which is also expressed in the hindlimb mesenchyme progenitor cells prior to the onset of hindlimb bud (Sun et al., 2007; Yang et al., 2006). *Isl1*-lineage cells occupy a majority of the hindlimb bud mesoderm with a posterior to anterior gradient, but do not contribute to ectoderm. *Isl1*-derived cells do not appear to contribute to the forelimb (Yang et al., 2006). Despite the embryonic lethality seen in *Bcor* $^{Fl/Y}$;*Isl1-Cre* embryos (Fig. 6A), we were able to examine embryonic hindlimb development in E14.5 and E15.5 mutants and found that deletion of *Bcor* within the *Isl1* lineage resulted in simple (cutaneous only, Fig. 6 N, P) or complex (involving the bone, Fig. 6 R, T) syndactyly of the second and third digits (Fig. 6 M–T). The syndactyly was observed in 4/17 of E 14.5 mutants but never in controls (0/75, Fig. 6 M, Q, O, S). We conclude that *Bcor* in the mesenchyme can play a role in hindlimb patterning.

Mutation of *Bcor* in extraembryonic lineages results in a reduced labyrinth, trophoblast giant cell expansion and midgestation lethality

Our previous studies suggested a likely requirement for *Bcor* in extraembryonic tissue development and/or function, based on a parent-of-origin effect. In brief, chimeric males carrying a hypomorphic *Bcor* ^{Neo} allele could produce viable heterozygous progeny, but females heterozygous for the same mutant allele could not (Wamstad et al., 2008). X chromosome inactivation in extraembryonic tissues of the mouse (in contrast to humans (Moreira de Mello et al., 2010)) depends on parental inheritance: the paternal X chromosome is selectively inactivated in trophectoderm and primitive endoderm, which give rise to many but not all extraembryonic cell lineages (the exceptions being the extraembryonic mesoderm and the amniotic ectoderm) (Takagi and Sasaki, 1975; West et al., 1977). Thus, the simplest explanation for the parent of origin effect is that the maternally inherited hypomorphic *Bcor* ^{Neo} allele was insufficient to support placental function, and therefore it could only be inherited as an inactivated paternal allele. In the *β-actin-Cre* crosses described above, we likewise found that OFCD newborns could only be recovered when the wild type X chromosome was maternally inherited and therefore active in extraembryonic tissues (*Bcor* $^{+(m)/\Delta E9-10(p)}$, Fig. 1F, left). Another genetic test also indicated an extraembryonic requirement for *Bcor:* live OFCD newborns were also produced by mating *Bcor* $^{Fl/Fl}$ females with males expressing *Sox2*-Cre, specifically targeting the inner cell mass (Hayashi et al., 2002). This result indicates that conditional deletion of *Bcor* in epiblast derived tissue is not lethal as long as there is a functional maternal allele in the extraembryonic tissue (data not shown).

To examine the role of *Bcor* in extraembryonic development, we again conditionally deleted *Bcor* using *β-actin-Cre*. However, in these crosses (Fig. 1F, right, *Bcor* $^{Fl/Fl}$ female mice crossed to *β-actin-Cre* males), the X chromosome with the wild type *Bcor* allele will be paternally derived (*Bcor* $^{\Delta E9-10/+(p)}$) and thus should be inactivated via XCI in the extraembryonic trophectoderm and primitive endoderm of female progeny. We first examined our *in situ* analysis of *Bcor* expression from this cross at E7.5 and E8.5 (Fig. 3) this time focusing on the females. Using a probe for exons 9 and 10, which are only present in the wild type and *Bcor* ^{Fl} alleles, we clearly saw paternal silencing of the wild type allele in the developing extraembryonic tissue at E7.5 and in the chorion at E8.5 in the *Bcor* $^{\Delta E9-10/+(p)}$ concepti (Fig. 3 C and G vs. D and H, arrow heads). However, there was some escape from XCI in the parietal-trophoblast giant cells (P-TGC) on the surface of the ectoplacental cone in the *Bcor* $^{\Delta E9-10/+(p)}$ concepti (Fig. 3 G vs. H, arrow). It has previously been reported that escape from XCI can occur in a gene-specific manner particularly in the endoreduplicated primary and secondary TGC (Corbel et al., 2013; Hadjantonakis et al., 2001), and our results indicated that *Bcor* is one of these genes. The *Bcor* $^{\Delta E9-10/+(p)}$ embryos themselves (Fig. 3D, H) show reduced *Bcor* exon 9 and 10 levels relative to *Bcor* $^{Fl/Y}$ and *Bcor* $^{Fl/+}$ controls (Fig. 3 A, C, E and G) due to mosaic XCI in the epiblast.

We next asked whether the mutant *Bcor* allele can support extraembryonic development when the wild type allele is silenced (or partially silenced in the case of the P-TGCs). Matings of the *Bcor* $^{Fl/Fl}$ females to *β-actin-Cre* males did not produce live born *Bcor* $^{\Delta E9-10/+(p)}$ pups. Examination of embryos from 21 litters of timed matings revealed that, at E8.5, *Bcor* $^{\Delta E9-10/+(p)}$ embryos were slightly smaller and had on average 2.8 fewer somites than their littermate controls. *Bcor* $^{\Delta E9-10/+(p)}$ embryos continued to show intrauterine growth restriction at E10.5 (Fig 7 A and B), and by visual inspection, placentae of *Bcor* $^{\Delta E9-10/+(p)}$ embryos appeared to have more blood relative to controls and the vast majority were dead by E12.5.

We sectioned placentae at E10.5 and E11.5 and found defects in trophectoderm-derived cell lineages in the placenta and parietal yolk sac (PYS) (Fig. 7 C–J). We find over-representation of larger than normal P-TGCs. Normally P-TGC form a single layer in the PYS and a single or near-single layer separating the spongiotrophoblasts (Sp-T) layer from the maternal decidua. The *Bcor* mutant P-TGC appear to invade the Sp-T layer and spread to form multiple layers in the PYS (Fig. 7 C–F, compare regions indicated by black arrows). This overrepresentation of P-TGC and likely Sp-T cells (Fig. 7 E–J, layer indicated by blue line) appears to be at the expense of the labyrinth layer, as it is thinner in placental midpoint sections (indicated by black line). Increased levels of maternal blood are also observed near the P-TGCs (Fig. 7 A and C vs. B and D, bright pink in H&E). These results suggest a skewing in the balance of trophoblast cell types, in particular the P-TGC and Sp-T cells. In summary, mutation of *Bcor* in extraembryonic lineages results in defective placental and PYS development that is not compatible with survival of the embryo.

Generation of a transgenic conditional *BcorA* expression allele

Bcor expression is non-uniform during embryonic development, with higher levels corresponding roughly to the tissues affected in OFCD patients (Wamstad and Bardwell,

2007). *Bcor* is also alternatively spliced into four isoforms (A-D) with isoform A including all possible coding sequences. To ask whether the pattern of expression and/or the isoform of *Bcor* is important for normal development, we generated a transgenic conditional *Bcor* expression allele using a knock-in approach. We inserted a conditional myc-tagged *BcorA* (*mBcorA*) expression cassette into the murine *Rosa26* locus, generating a $Rosa26^{LsLmBcorA}$ allele (Fig. 8 A and B). Expression of Cre recombinase excises the LoxP-flanked *Neo* resistance "stop" cassette (*LsL*), allowing expression of the *mBcorA* coding sequence.

We bred female $Rosa26^{LsLmBcorA/\,LsLmBcorA}$ mice with *β-actin-Cre* male mice (Lewandoski et al., 1997) to generate $Rosa26^{LsLmBcorA/+}$;*β-actin-Cre* ($Rosa26^{mBcorA/+}$) and $Rosa26^{LsLmBcorA/+}$ (control) animals. *In situ* analysis of E8.5 $Rosa26^{mBcorA/+}$ vs. control concepti (Fig. 8C) revealed ubiquitous and higher levels of *Bcor* expression particularly in the embryo. Where examined, BCOR has been found by ChIP-seq to bind its own promoters in human and mouse cells (Hatzi et al., 2013; Huang et al., 2013; Kotov et al., 2019; Wang et al., 2018), so to determine the effect of the transgenic allele on expression we isolated E9.5 embryos and placentae from four individual concepti ($Rosa26^{mBcorA/+}$ and control) and extracted RNA and protein for qRTPCR and western blot analysis. We found that in the embryo the endogenous transcript was repressed 4-fold while the overall expression of *Bcor* was doubled in $Rosa26^{mBcorA/+}$ (Fig. 8D). In the placenta, the endogenous transcript appeared to be reduced slightly but overall transcript levels were unaffected in $Rosa26^{mBcorA/+}$. These results were confirmed by western analysis using antibodies to BCOR and the myc-tag. Increased levels of BCOR in the embryo were derived mainly from the slightly larger mBCORA protein (Fig. 8E). In the placenta, a mix of endogenous BCOR and mBCORA was observed. In summary, *Bcor* expression was less affected by the transgene in the placenta than in the embryo proper where *Bcor* was negatively autoregulated and transgene activation largely substituted an increased and ubiquitous expression of A isoform of BCOR for the mixture of isoforms normally expressed (BCORC>BCORD>BCORA (Wamstad and Bardwell, 2007)).

Mis-expression of *BcorA* during development results in midgestation lethality

To determine whether ubiquitous and high level of expression of *mBcorA* mRNA disrupts embryonic development, we genotyped newborns and recovered 62 $Rosa26^{LsLmBcorA/+}$ pups. Although an equal number of $Rosa26^{mBcorA/+}$ pups were predicted, none were recovered, indicating that overexpression of *BcorA* is lethal. We next dissected litters from pregnant dams at various embryonic time points to determine the age of death. At E10.5, the earliest time point examined, equal numbers of live $Rosa26^{mBcorA/+}$ and control, $Rosa26^{LsLmBcorA/+}$, embryos were present but over the next 3 days the fraction of $Rosa26^{mBcorA/+}$ decreased, such that by E14.5 no live $Rosa26^{mBcorA/+}$ embryos were found (Fig. 8F). Examination of live E10.5 - E13.5 $Rosa26^{LsLmBcorA/+}$ control (Fig. 8 G, I, K, M) vs. $Rosa26^{mBcorA/+}$ experimental (Fig. 8 H, J, L, N) concepti revealed grossly normal yolk sacs and placentae but increasingly abnormal fetuses. In particular, the hindbrain was more bulbous throughout the period examined, by E12.5 the snout and mandible were shortened and misshapen, by E12.5 the eyes were misshapen, and by E13.5 there were multiple examples of small and misshapen forelimbs. We conclude that proper regulation of *Bcor* expression is required for fetal development and embryonic viability past E13.5.

Discussion

Vertebrates have multiple PRC1 complexes of varied composition, and in-depth understanding of their specific roles in embryonic development remains limited. Untangling the functions of individual PRC1 complexes in different tissues during development requires conditional genetics, targeting complex-specific components with temporal and cell-type specificity. Here we undertook both conditional knockout and overexpression approaches to better understand the developmental roles of PRC1.1 complex(es) containing BCOR. This complex is of particular interest because *BCOR* mutations are found in human syndromes and multiple cancer types. Our mouse mutant not only successfully models multiple OFCD-related phenotypes, including those of ocular, craniofacial, skeletal and cardiac tissues, but also revealed unexpected findings, such as presence of ectopic salivary glands, the etiology of the cleft palate phenotype, and occurrence of lethal placental developmental defects. Together our analyses illuminate multiple roles played by BCOR-PRC1.1 complex(es) during embryonic and fetal development and offer possible explanations for the rarity of OFCD syndrome patients.

Modeling OFCD in the mouse

In our analysis of heterozygous OFCD female mice (*Bcor* $^{+/\Delta E9-10\,(p)}$), we found variable expressivity of multiple phenotypes, consistent with mosaic expression of the mutant allele due to X inactivation (Lyon, 1961; Tan et al., 1993). Many of these phenotypes, including palatal clefting, cataracts, microphthalmia and ptosis are coincident with known OFCD patient phenotypes. On a mainly 129S1:C57BL/6N mixed genetic background, we had a ~50% reduction in postnatal viability of the OFCD females relative to controls, likely due to palatal clefting and cardiac defects. In contrast, on the C57BL/6N background, survival of OFCD females at weaning was only ~5% relative to controls, indicating that genetic modifiers must exist. Male patients with *BCOR* loss-of-function mutations are never found. In our analysis of *Bcor* $^{\Delta E9-10/Y}$ embryos, development was delayed by approximately half a day, based on somite numbers, embryonic turning was never completed, and death occurred at or before E9.25. The forebrain was reduced in size and, consistent with this reduction, *Otx2*, *Fgf8* and *Foxg1* expression was reduced. Although we did not examine cardiac development in the *Bcor* $^{\Delta E9-10/Y}$ mutants, in somite-matched embryos, the trunk region was reduced in size, suggesting that heart development is affected. A previous study examined ES cell aggregation embryos generated from 3 different gene-trap lines, one in intron 1c (P101H07) and two in intron 5 (DB0053 and XE541). The phenotype of the P101H07-derived embryos is described as exhibiting exencephaly and patterning and turning defects ((Cox et al., 2010) and MGI:3897494), which is reminiscent of our *Bcor* $^{\Delta E9-10/Y}$ phenotypes, although we have not observed exencephaly *per se*. In contrast, the phenotype of the DB0053- and XE541-derived embryos is more severe than that of *Bcor* $^{\Delta E9-10/Y}$ mutants in that posterior truncation of the embryos and a failure of chorioallantoic fusion was observed. Based on our previous work with XE541 ES cells, we know that very high levels of a BCORΔE6–15/βgeo fusion protein are produced by this allele relative to wild type levels of BCOR (Fig. 2C in (Wamstad et al., 2008)). In addition, the pattern of LacZ staining does not completely mirror our *Bcor in situ* analyses. Thus, the more severe phenotype of XE541-derived embryos may be due to a dominant effect of the

overexpression/misexpression of the BCORΔE6–15/βgeo fusion protein, whereas our *Bcor* $^{\Delta E9-10}$ allele leads to reduced levels of a truncated protein (Fig 1D) and is predicted to cause severe loss-of-function. Alternatively, the strain background may affect the severity of the phenotype, as both DB0053 and XE541 are on the 129P2/OlaHsd background and most of our studies employed a mixed mainly 129S1:C57BL/6N background.

Roles of PRC1.1 in development

Because BCOR is found in a subset of PRC1 complexes, one might expect that the *Bcor* loss-of-function phenotype would be milder or more selective than those involving more universal PRC1 components, such as *Rnf2 (Ring1b)*. Indeed, a previous knockout study targeting *Rnf2* found that mutant embryos arrest during gastrulation and do not progress to the head fold stage or lay down somites (Voncken et al., 2003). This earlier developmental arrest relative to that of *Bcor* $^{\Delta E9-10/Y}$ concepti suggests that at least one other PRC1 complex is required in development prior to the BCOR containing PRC1.1 complex. PCGF1, which appears specific to PRC1.1, binds both RNF2 and BCOR in PRC1.1. A *Pcgf1* knockout was generated and analyzed at E9.5 by the International Mouse Phenotyping Consortium (https://www.mousephenotype.org/data/genes/MGI:1917087). Similar to *Bcor* $^{\Delta E9-10/Y}$ mutants, the *Pcgf1* homozygotes exhibit growth retardation, abnormal turning, and abnormal brain and cardiac development. *Pcgf1* mutants are viable at E9.5 but die by E12.5, the next time examined. A more detailed comparison of the phenotypes could reveal additional differences, but in terms of lethality the *Bcor* mutant appears more severe, suggesting that the essential role(s) of BCOR in development is slightly earlier than that of PCGF1. Since PCGF3 has been shown to bind BCOR *in vitro*, it is possible that PCGF1 and PCGF3 perform some redundant roles *in vivo*, potentially explaining the later lethality of *Pcgf1* mutants. KDM2B, another PRC1.1 component, helps target the complex to CpG islands (Farcas et al., 2012; He et al., 2013; Wu et al., 2013). A *Kdm2b* mutant that disrupts all mRNA isoforms (Boulard et al., 2015) has an open and malformed anterior neural tube, a kinked and tortuous posterior neural tube, abnormal somitogenesis, heart defects, and reduced size, and did not develop past embryonic day E10.5. The overlapping yet distinct phenotypes and later death than *Bcor* $^{\Delta E9-10/Y}$ embryos suggest that the two proteins have correspondingly overlapping and distinct roles in development. Together these observations suggest a common midgestational requirement for the PRC1.1 complex with a degree of functional divergence and specialization among individual PRC1.1 components.

Bcor in craniofacial and limb development

Removing *Bcor* from the neural crest cell lineage using *Pax3-Cre* or *Wnt1-Cre* revealed a requirement for *Bcor* in palatogenesis between E13.5 and E15.5. However, because mutant palatal shelves grown in culture could elevate and fuse properly, we conclude that the defect is secondary to a defect outside of the palate. Proper elevation of palatal shelves requires depression of the tongue within the oral cavity to create space, closely linking palate formation to mandibular development (Barrow and Capecchi, 1999; Diewert, 1981; Huang et al., 2008; Lavrin et al., 2001; Yu and Ornitz, 2011). The tongue appeared to remain elevated in mutants, possibly due to tongue dysmorphogenesis and/or ankyloglossia, reduced mandibular size, and/or ectopic salivary glands, potentially explaining the failure in palatal shelf elevation. The mandibular defects, in turn, are likely a consequence of

the malformation of Meckel's cartilage, which we observed at E14.5. The patterning and growth of Meckel's cartilage involves the coordinated interplay between multiple signaling molecules in the ectodermal and the mesenchymal compartments. These include FGF8, BMP4, WNT, and SHH, with SHH being a key outgrowth signal (Li et al., 2017; Parada and Chai, 2015). Meckel's cartilage first lengthens ventromedially and dorsolaterally on both sides and fuses at the most distal tip (Ramaesh and Bard, 2003; Richany et al., 1956). Thus, perhaps the *Bcor* mutant neural crest-derived mesenchyme cannot respond to signaling from the epithelium or it is impaired in its ability to proliferate. *Sox9* is important for chondrogenesis and *Sox9* heterozygotes have similarly abnormally shaped Meckel's cartilage and cleft palates (Bi et al., 2001) so another possibility is that *Sox9* expression is indirectly affected by *Bcor* loss-of-function. As mentioned earlier, cleft palate in OFCD patients is sometimes associated with bifurcations of the uvula and tongue, and although we did not specifically score bifurcation of the tongue, we did observe it in occasional *Bcor* mutants (not shown). Our data suggest that the cleft or high-arched palate found in 29% of OFCD patients (Hilton et al., 2008; Hilton et al., 2009; Ragge et al., 2018) may be related to the observed small or asymmetric mandibles or perhaps undiagnosed tongue dysmorphology or ectopic salivary glands.

Mutation of *Bcor* in the neural crest lineage also resulted in shortening of the tympanic ring from the dorsal side and thickening of the remaining structure. This tympanic ring phenotype is very similar to that seen in a neural crest-specific deletion of *Nr2f2* and a *Tshz1* mutant (Core et al., 2007; Hsu et al., 2017). The tympanic ring normally supports the tympanic membrane and encloses part of the middle ear (Hasso et al., 1995). Thus defects in this structure might contribute to the mild conductive hearing loss observed in some OFCD patients (Hilton et al., 2008; Hilton et al., 2009; O'Byrne et al., 2017; Ragge et al., 2018).

Deletion of *Bcor* in *Isl1*-expressing cells caused simple or complex syndactyly of the second and third hindlimb digits. Thirty-three percent of OFCD patients have 2–3 toe syndactyly although reports do not specify whether it is simple or complex (Ragge et al., 2018). *Hox* genes are well known targets of the Polycomb system. If BCOR containing PRC1.1 indeed represses specific *Hox* genes, mutation of *Bcor* would lead to upregulation of these genes, and many studies have shown that *Hox* gene misexpression affects patterning of structures including the distal limbs (Mallo, 2018; Perez-Gomez et al., 2018). A recent review (Al-Qattan, 2019) suggests that a three-step pathway of pathogenesis for syndactyly potentially explains nearly all types of syndactyly. This pathway includes overactivation of the WNT canonical pathway or the suppression of the BMP canonical pathway, leading to overexpression of FGF8 and suppression of retinoic acid signaling, and ultimately suppression of both apoptosis and extracellular matrix (ECM) degradation. We speculate that mutation of *Bcor* may affect this pathway through increased expression of *Wnts* or *Fgf8*.

Bcor in salivary gland development

Bcor neural crest cell conditional mutants had a pair of ectopic major salivary glands located in an area delimited by three muscles, the hyoglossus superiorly, the mylohyoid inferiorly, and the genioglossus on the lingual side. Excretory ducts of the SM and SL glands normally travel through the buccal side of this anatomical region. Interestingly, these ectopic SGs

drained into the oral cavity through a separate set of excretory ducts that ran alongside the SM and SL gland excretory ducts on the lingual side. This independent ductal system suggests that the ectopic SG tissue represents true heterotopic SCs (supernumerary glands) rather than accessory glands (lobes of SG tissue draining into the ducts of existing major glands). Furthermore, although these ectopic SGs were predominantly serous, localised groups of mucous acini could be found, suggesting that they are neither SM- nor SL-like SGs and therefore distinct from the normal SG group found in the lower jaw.

To date, the genetic control of SG initiation is poorly understood in mammals. Although retinoic acid signalling is required for initiation of SG development, it is unknown whether activation of this pathway is sufficient to induce a salivary gland fate (Metzler et al., 2018). *Bcor* mutants are the first example of a mouse mutant developing a supernumerary pair of major SGs in an ectopic location, and as such, their study will enable a new avenue of research to identify molecular cues that determine the sites of SG development in mammals. The sufficiency of neural crest *Bcor* mutation in inducing ectopic SG formation also points to BCOR as a major negative regulator of SG initiation and suggests targeted *Bcor* suppression in adult tissues as a potential basis for SG regenerative therapy. However, we caution that *BCOR* mutations have been found in ~10% of adenoid cystic carcinomas of salivary glands (Ho et al., 2019; Morris et al., 2017), suggesting that BCOR may function as a tumor suppressor protein in this context.

Bcor in cardiac development

Deletion of *Bcor* in the *Isl1*-expressing cell lineage caused embryonic lethality with the vast majority of animals dying between E15.5 and E18.5 and none surviving to weaning. We observed incompletely penetrant cardiac outflow tract and ventricular septal defects in mutant embryos, in particular PTA and VSD. Conoventricular VSD is often a consequence of PTA, as the proximal outflow tract cushions fail to properly form the subpulmonary and subaortic infundibulum (Conway et al., 2003) so the PTA may be the primary defect. This suggests a key role for *Bcor* in the *Isl1*-expressing lineage for outflow tract septation. In addition, we observed at low penetrance both interruption of the aortic arch and right-sided aortic arch, suggesting a role for *Bcor* in aortic arch artery patterning. This is consistent with the expression pattern of *Isl1* in aortic arch artery smooth muscle (Sun et al., 2007).

The absence of defects in outflow tract septation and aortic arch artery remodeling when we deleted *Bcor* with the *Pax3-Cre* suggests that the requirement for *Bcor* lies in *Isl1*-expressing SHF cells, rather than in neural crest cells themselves. This does not, however, necessarily exclude a cell non-autonomous effect on cardiac neural crest cell progenitors, an area which must undergo further investigation in future studies. We did not observe lethality when we deleted *Bcor* with other *Cre* alleles including *Nkx2.5-Cre, Nkx2.5-IRES-Cre* and *xMlc2-Cre* (Moses et al., 2001; Stanley et al., 2002) (Breckenridge et al., 2007). *Isl1* and *Nkx2.5* are co-expressed in early cardiac progenitors that give rise to multiple cardiac cell types including some of the cell types contributing to the outflow tract, so it is surprising that conditional *Bcor* mutation with *Nkx2.5-Cre* alleles resulted in viable animals. This differing effect on cardiac phenotypes may be explained by distinct timing of *Isl1* and *Nkx2.5* expression, with *Isl1* expressed primarily in progenitors, where *Bcor* deletion may be critical, while

Nkx2.5 expression is maintained at lower levels even as cells differentiate (Komuro and Izumo, 1993; Prall et al., 2007). In addition, the efficiency of CRE deletion with *Isl1-Cre* vs. *Nkx2.5-Cre* can be locus-specific (Ma et al., 2008) and efficient deletion in precursors to the outflow tract may be required to produce PTA. Thus, inefficient deletion may also explain the absence of lethality observed using some of the other *Cre* alleles. Since we did not carry out an in-depth analysis of conditional *Bcor* deletion animals with *Cre* alleles other than *Isl1-Cre,* we cannot exclude the possibility that these animals had non-lethal cardiovascular defects.

Given the incomplete penetrance of the PTA, we also considered the alternative explanation that heart defects might be secondary to placental defects. Placental defects correlate strongly with abnormal brain, heart and vascular development in mice (Perez-Garcia et al., 2018), and *Isl1*-expressing progenitors from the allantois contribute to the umbilical vessels and their interface with the placenta (Keenan et al., 2012; Zhuang et al., 2013). In addition, fetal endothelial cells in the labyrinth, which derive from the allantois, are labelled in *Isl1-Cre* concepti harboring the Ai14 version of a *TdTomato-Cre* reporter (Madisen et al., 2010) (data not shown). Furthermore, *Bcor* is expressed in the allantois (Fig. 3 E, G) and *in vitro* knockdown of *BCOR* induces endothelial sprouting (Buchberger et al., 2017). We therefore examined $Bcor^{Fl/Y}$;*Isl1-Cre* placentae but found no obvious defects in the E12.5 labyrinth (data not shown) suggesting the cardiac defects are not due to mutation of *Bcor* in the umbilical cord or fetal endothelial cells interfacing with the placenta. We conclude that mutation of *Bcor* in *Isl1* lineage cells, most likely those in the heart, contributes to PTA and VSD. However, since *Isl1-Cre* is a knock-in allele, we cannot discount the possibility that *Isl1* heterozygosity also contributes to the phenotype in $Bcor^{Fl/Y}$;*Isl1-Cre* mutants, even though heterozygous *Isl1* animals have no cardiac phenotypes (Pfaff et al., 1996). The observed PTA and VSD, together with the most common cardiovascular phenotypes of OFCD patients, suggest that *Bcor* plays a key role in *Isl1*-expressing progenitors for proper septation of the right ventricular outflow tract.

Based on the work described here as well as previous studies, both canonical and non-canonical PRC1 complexes are involved in cardiac development. As mentioned above, mutation of *Rnf2* results in early embryonic lethality, but while this developmental arrest can be partially rescued by loss of the cell cycle regulator *Cdkn2a*, cardiac tissue does not develop in the double-knockout animals, indicating a critical early role for PRC1 in cardiac development. Previous loss-of-function studies of *Phc1*, encoding a component of the canonical PRC1.2 and PRC1.4 complexes, gave overlapping and distinct cardiac phenotypes relative to those we observed in *Bcor* mutants. Embryo-wide deletion of *Phc1* caused failure of cardiac looping and a high percentage of atrial or ventricular septation defects with age (Shirai et al., 2002; Takihara et al., 1997). Whether *Bcor* and thus the non-canonical PRC1.1 plays additional roles in cardiac development will require further studies, including a detailed examination of emerging cardiac structures in $Bcor^{\Delta E9-10/Y}$ and cell-type specific mutants. Since OFCD patients can have ASD as well as VSD, double outlet right ventricle, and patent ductus arteriosus, it is possible these other cardiac defects can be modeled using appropriate *Cre* alleles.

Bcor in placental development

We found that depletion of a functional *Bcor* allele from trophoblast-derived tissues and primitive endoderm is incompatible with survival of the fetus. Both the PYS and the placenta exhibited defects including over-representation of larger than normal P-TGCs, which appear to invade the Sp-T layer and spread to form multiple layers in the PYS. The Sp-Ts also appeared overrepresented while the labyrinth was thinner. Although we have not determined the exact cause of fetal lethality, obvious candidates include insufficient nutrient and oxygen exchange due to the smaller labyrinth and excessive hormone secretion by the vast excess of P-TGCs. The skewing in the balance of trophectoderm-derived cell types that we observed *in vivo* contrasts with *in vitro* studies in which *Bcor* was knocked down (Zhu et al., 2015a) or mutated (our unpublished work) in cultured trophoblast stem cells. In these studies, *Bcor* depletion/mutation skewed the differentiation of trophoblast stem cells towards syncytiotrophoblast at the expense of spongiotrophoblast and P-TGCs. This difference may be due to absence of *in vivo* factors that can influence cell fate specification. Alternatively, since we showed that in P-TGCs *Bcor* undergoes at least some escape from XCI, this may affect the phenotypic outcome. Further work is therefore needed to understand how BCOR can influence trophoblast differentiation and what factors may be acting *in vivo* to influence cell fate specification.

Insights into the rarity of OFCD

Fewer than 100 human females with OFCD have been reported (Hilton et al., 2009; Ng et al., 2004; Ragge et al., 2018; Suzumori et al., 2013), indicating OFCD is an extremely rare single-gene X-linked dominant syndrome. However, in non-lethal single-gene dominant syndromes (X-linked or autosomal), spontaneous mutations typically present at about 1:10,000 to 1:40,000 (Nicholas, 2003). The discrepancy between the observed and the expected frequencies of OFCD patients is likely multifactorial and our studies have shed some light on this discrepancy. Possible causes include prenatal lethality, death before diagnosis, and incomplete diagnosis. With respect to prenatal lethality, given the essential role of *Bcor* in mouse placental development, we suggest that placental defects may be a major contributor. In contrast to the paternal X-inactivation found in mice, in humans the extra-embryonic tissue of female concepti undergoes clonal random X-inactivation (Moreira de Mello et al., 2010), and thus mutant *BCOR* alleles are expressed in a mosaic fashion. In some cases we presume there is sufficient placental function for the OFCD fetus to survive, but in others the vagaries of X-inactivation, which can be extreme (Wu et al., 2014), likely result in placental insufficiency and preterm lethality. Importantly miscarriages are reported in OFCD females (McGovern et al., 2006; Sujatha and Namita, 2008; Wilkie et al., 1993), consistent with placental insufficiency. Similarly, there are only five reports of mother-to-daughter OFCD transmission, and one involved IVF to treat infertility (Hedera and Gorski, 2003; Kondo et al., 2012; Lozic et al., 2012; McGovern et al., 2006). Collectively these data suggest that *BCOR* $^{+/-}$ mutations can affect placental development and are likely responsible for some unexplained cases of miscarriage, which may contribute to the rarity of OFCD patients. Prenatally we also observed some loss of *Bcor* $^{Fl/+}$;*Isl1-Cre* embryos, suggesting cardiac defects could account for some prenatal loss of OFCD females. With respect to death before diagnosis, our studies indicate that genetic modifiers, cardiac defects and cleft palate defects can affect early survival of OFCD mice and thus could also contribute to the rarity

of OFCD in humans. Finally, the variable expressivity of OFCD phenotypes due to mosaic expression of the mutant X chromosome likely means that more OFCD patients exist in the population but only have mild and therefore undiagnosed phenotypes.

Over/misexpression of *BcorA*

There are several possible molecular explanations for the craniofacial and limb phenotypic abnormalities resulting from inappropriate *BcorA* expression. First, replacing the normal mix of BCOR isoforms with just the A isoform may cause gain or loss of specific BCOR activities in sensitive tissues. For example, although we do not yet know the significance, BCORA but not BCORC can interact with AF9 (Srinivasan et al., 2003), a protein with a YEATS domain that can recognize histone crotonylation (Li et al., 2016). Second, elevated expression of the A isoform may disrupt the activity of BCOR-containing complexes in one of two ways: inappropriate BCOR expression could increase the amount and thus the activity of complexes containing BCOR; alternatively, it could disrupt these complexes by causing incomplete complex formation due to titration of limiting subunits. Either way, these results indicate that the differential expression of *Bcor* mRNAs in different tissues is important for its normal developmental function.

Other studies using the *Bcor* $^{\Delta E9-10}$ *and Rosa26*^{mBcorA} alleles

During the course of this study we also collaborated with several laboratories to help dissect the roles of *Bcor* in normal immune system development and cancer using the *Bcor* alleles that are first fully described here. These collaborations revealed additional functions for *Bcor*. Within the B cell lineage, *Bcor* is required for germinal center (GC) formation and BCL6/*Ezh2*^{Y641F} driven lymphomagenesis (Beguelin et al., 2016). Within the T cell lineages, BCOR is critical for optimal GC-Tfh cell differentiation and contributes CD4^{+} T helper 17 cell formation (Kotov et al., 2019; Yang et al., 2015). In addition, mice with bone marrow reconstituted with *Bcor* $^{\Delta E9-10/Y}$ cells developed lethal T-ALL (Tara et al., 2018). These mice harboring *Bcor* $^{\Delta E9-10/Y}$ bone marrow were more severely affected than those harboring a *Bcor* $^{\Delta E4/Y}$ allele (Tanaka et al., 2017), suggesting that *Bcor* $^{\Delta E9-10/Y}$ is a strong loss-of-function allele and *Bcor* $^{\Delta E4/Y}$ is hypomorphic. Within the myeloid compartment, multiple lines of evidence using the *Bcor* $^{\Delta E9-10}$ *and Rosa26*^{mBcorA} alleles demonstrated that *Bcor* mutation perturbs myeloid differentiation and that *Bcor* can function as a tumor suppressor gene (Cao et al., 2016; Kelly et al., 2019; Tara et al., 2018). Outside the immune system, *Bcor* $^{\Delta E9-10}$, combined with loss of the SHH-receptor gene *Ptch1*, resulted in highly penetrant medulloblastomas, again demonstrating that *Bcor* functions as a tumor suppressor (Kutscher et al., 2020). These studies, together with the documented *BCOR* mutations in a variety of cancers, plus the report of an OFCD patient with T cell lymphoma, suggest that OFCD patients may have elevated risk of cancer development.

This study has defined developmental requirements and gene regulatory functions for *Bcor* in several embryonic tissues whose development is affected in OFCD patients, providing insight into the basis of OFCD. Conditional gene targeting allowed us to examine the effects of complete *Bcor* loss in specific lineages, avoiding confounding effects of functional mosaicism due to X inactivation, as in OFCD patients. We suggest that the *Bcor* ^{Fl} mouse may provide a useful model to identify and test genes and pathways whose

targeted reduction could aid therapy of OFCD and other PRC1.1-related human pathologies. Furthermore, it is proving to be very useful in cancer research, where loss-of-function mutations in BCOR can drive tumorigenesis.

Acknowledgements

We thank Yasuhiko Kawakami, Anna Petryk, David Zarkower, Wendy Dean, Michael O'Connor and members of the Bardwell lab for discussion and advice, the Copeland/Jenkins lab for recombineering reagents and Charles Hemenway for a mouse *Bcor* cDNA clone. We also thank Y. Kawakami, Y. Nakagawa, and J Rossant for *in situ* probes, M. Lewandoski, S. Evans, E. Olson, R. Harvey, T. Mohun and J. Rossant for mice and L. Gammill and D. Garry for reagents. We thank Colleen Forster and the BLS Histology and IHC Laboratory for some tissue processing and histology advice and assistance. This work was supported by funding from the National Institutes of Health 5R01HD084459 and 5R01CA071540 (VJB), 5F30HL093996 (MYH), 5T32DE007288 (JAW), and 5T32GM008244 (MYH), the American Heart Association 0810194Z (MYH), the University of Minnesota Wetzel Fund (MYH), Graduate School, Minnesota Masonic Charities, and Office of the Vice President for Research (VJB) and the UK Medical Research Council (PTS) MR/K011421/1/MRC_/Medical Research Council/United Kingdom.

REFERENCES

Abbott BD, 2003. Organ culture of midfacial tissue and secondary palate. Curr Protoc Toxicol Chapter 13, Unit13 16.

Adams DJ, Quail MA, Cox T, van der Weyden L, Gorick BD, Su Q, Chan WI, Davies R, Bonfield JK, Law F, Humphray S, Plumb B, Liu P, Rogers J, Bradley A, 2005. A genome-wide, end-sequenced 129Sv BAC library resource for targeting vector construction. Genomics 86, 753–758. [PubMed: 16257172]

Al-Qattan MM, 2019. A Review of the Genetics and Pathogenesis of Syndactyly in Humans and Experimental Animals: A 3-Step Pathway of Pathogenesis. Biomed Res Int 2019, 9652649. [PubMed: 31637260]

Aloia L, Di Stefano B, Di Croce L, 2013. Polycomb complexes in stem cells and embryonic development. Development 140, 2525–2534. [PubMed: 23715546]

Anderson JP, Dodou E, Heidt AB, De Val SJ, Jaehnig EJ, Greene SB, Olson EN, Black BL, 2004. HRC is a direct transcriptional target of MEF2 during cardiac, skeletal, and arterial smooth muscle development in vivo. Mol Cell Biol 24, 3757–3768. [PubMed: 15082771]

Ang SL, Conlon RA, Jin O, Rossant J, 1994. Positive and negative signals from mesoderm regulate the expression of mouse Otx2 in ectoderm explants. Development 120, 2979–2989. [PubMed: 7607086]

Astolfi A, Melchionda F, Perotti D, Fois M, Indio V, Urbini M, Genovese CG, Collini P, Salfi N, Nantron M, D'Angelo P, Spreafico F, Pession A, 2015. Whole transcriptome sequencing identifies BCOR internal tandem duplication as a common feature of clear cell sarcoma of the kidney. Oncotarget 6, 40934–40939. [PubMed: 26516930]

Barrow JR, Capecchi MR, 1999. Compensatory defects associated with mutations in Hoxa1 restore normal palatogenesis to Hoxa2 mutants. Development 126, 5011–5026. [PubMed: 10529419]

Beguelin W, Teater M, Gearhart MD, Calvo Fernandez MT, Goldstein RL, Cardenas MG, Hatzi K, Rosen M, Shen H, Corcoran CM, Hamline MY, Gascoyne RD, Levine RL, Abdel-Wahab O, Licht JD, Shaknovich R, Elemento O, Bardwell VJ, Melnick AM, 2016. EZH2 and BCL6 Cooperate to Assemble CBX8-BCOR Complex to Repress Bivalent Promoters, Mediate Germinal Center Formation and Lymphomagenesis. Cancer Cell 30, 197–213. [PubMed: 27505670]

Bi W, Huang W, Whitworth DJ, Deng JM, Zhang Z, Behringer RR, de Crombrugghe B, 2001. Haploinsufficiency of Sox9 results in defective cartilage primordia and premature skeletal mineralization. Proc Natl Acad Sci U S A 98, 6698–6703. [PubMed: 11371614]

Boulard M, Edwards JR, Bestor TH, 2015. FBXL10 protects Polycomb-bound genes from hypermethylation. Nat Genet 47, 479–485. [PubMed: 25848754]

Breckenridge R, Kotecha S, Towers N, Bennett M, Mohun T, 2007. Pan-myocardial expression of Cre recombinase throughout mouse development. Genesis 45, 135–144. [PubMed: 17334998]

Buchberger E, Payrhuber D, El Harchi M, Zagrapan B, Scheuba K, Zommer A, Bugyik E, Dome B, Kral JB, Schrottmaier WC, Schabbauer G, Petzelbauer P, Groger M, Bilban M, Brostjan C, 2017. Inhibition of the transcriptional repressor complex Bcl-6/BCoR induces endothelial sprouting but does not promote tumor growth. Oncotarget 8, 552–564. [PubMed: 27880939]

Buchwald G, van der Stoop P, Weichenrieder O, Perrakis A, van Lohuizen M, Sixma TK, 2006. Structure and E3-ligase activity of the Ring-Ring complex of polycomb proteins Bmi1 and Ring1b. Embo J 25, 2465–2474. [PubMed: 16710298]

Cai J, Kwak S, Lee JM, Kim EJ, Lee MJ, Park GH, Cho SW, Jung HS, 2010. Function analysis of mesenchymal Bcor in tooth development by using RNA interference. Cell Tissue Res 341, 251–258. [PubMed: 20563598]

Cao Q, Gearhart MD, Gery S, Shojaee S, Yang H, Sun H, Lin DC, Bai JW, Mead M, Zhao Z, Chen Q, Chien WW, Alkan S, Alpermann T, Haferlach T, Muschen M, Bardwell VJ, Koeffler HP, 2016. BCOR regulates myeloid cell proliferation and differentiation. Leukemia 30, 1155–1165. [PubMed: 26847029]

Cao R, Tsukada Y, Zhang Y, 2005. Role of Bmi-1 and Ring1A in H2A ubiquitylation and Hox gene silencing. Mol Cell 20, 845–854. [PubMed: 16359901]

Chai Y, Jiang X, Ito Y, Bringas P Jr., Han J, Rowitch DH, Soriano P, McMahon AP, Sucov HM, 2000. Fate of the mammalian cranial neural crest during tooth and mandibular morphogenesis. Development 127, 1671–1679. [PubMed: 10725243]

Chai Y, Maxson RE Jr., 2006. Recent advances in craniofacial morphogenesis. Dev Dyn 235, 2353–2375. [PubMed: 16680722]

Connelly KE, Dykhuizen EC, 2017. Compositional and functional diversity of canonical PRC1 complexes in mammals. Biochim Biophys Acta 1860, 233–245.

Conway SJ, Kruzynska-Frejtag A, Kneer PL, Machnicki M, Koushik SV, 2003. What cardiovascular defect does my prenatal mouse mutant have, and why? Genesis 35, 1–21. [PubMed: 12481294]

Corbel C, Diabangouaya P, Gendrel AV, Chow JC, Heard E, 2013. Unusual chromatin status and organization of the inactive X chromosome in murine trophoblast giant cells. Development 140, 861–872. [PubMed: 23362347]

Core N, Caubit X, Metchat A, Boned A, Djabali M, Fasano L, 2007. Tshz1 is required for axial skeleton, soft palate and middle ear development in mice. Dev Biol 308, 407–420. [PubMed: 17586487]

Cox BJ, Vollmer M, Tamplin O, Lu M, Biechele S, Gertsenstein M, van Campenhout C, Floss T, Kuhn R, Wurst W, Lickert H, Rossant J, 2010. Phenotypic annotation of the mouse X chromosome. Genome Res 20, 1154–1164. [PubMed: 20548051]

Damm F, Chesnais V, Nagata Y, Yoshida K, Scourzic L, Okuno Y, Itzykson R, Sanada M, Shiraishi Y, Gelsi-Boyer V, Renneville A, Miyano S, Mori H, Shih LY, Park S, Dreyfus F, Guerci-Bresler A, Solary E, Rose C, Cheze S, Prebet T, Vey N, Legentil M, Duffourd Y, de Botton S, Preudhomme C, Birnbaum D, Bernard OA, Ogawa S, Fontenay M, Kosmider O, 2013. BCOR and BCORL1 mutations in myelodysplastic syndromes and related disorders. Blood.

Danda S, van Rahden VA, John D, Paul P, Raju R, Koshy S, Kutsche K, 2014. Evidence of Germline Mosaicism for a Novel BCOR Mutation in Two Indian Sisters with Oculo-Facio-Cardio-Dental Syndrome. Mol Syndromol 5, 251–256. [PubMed: 25337074]

Danielian PS, Muccino D, Rowitch DH, Michael SK, McMahon AP, 1998. Modification of gene activity in mouse embryos in utero by a tamoxifen-inducible form of Cre recombinase. Curr Biol 8, 1323–1326. [PubMed: 9843687]

Depew MJ, 2008. Analysis of skeletal ontogenesis through differential staining of bone and cartilage. Methods Mol Biol 461, 37–45. [PubMed: 19030790]

Di Carlo V, Mocavini I, Di Croce L, 2019. Polycomb complexes in normal and malignant hematopoiesis. J Cell Biol 218, 55–69. [PubMed: 30341152]

Di Stefano C, Lombardo B, Fabbricatore C, Munno C, Caliendo I, Gallo F, Pastore L, 2015. Oculo-facio-cardio-dental (OFCD) syndrome: the first Italian case of BCOR and co-occurring OTC gene deletion. Gene 559, 203–206. [PubMed: 25620158]

Diewert VM, 1981. Correlation between alterations in Meckel's cartilage and induction of cleft palate with beta-aminoproprionitrile in the rat. Teratology 24, 43–52. [PubMed: 7302872]

Du R, Dinckan N, Song X, Coban-Akdemir Z, Jhangiani SN, Guven Y, Aktoren O, Kayserili H, Petty LE, Muzny DM, Below JE, Boerwinkle E, Wu N, Gibbs RA, Posey JE, Lupski JR, Letra A, Uyguner ZO, 2018. Identification of likely pathogenic and known variants in TSPEAR, LAMB3, BCOR, and WNT10A in four Turkish families with tooth agenesis. Hum Genet 137, 689–703. [PubMed: 30046887]

Elderkin S, Maertens GN, Endoh M, Mallery DL, Morrice N, Koseki H, Peters G, Brockdorff N, Hiom K, 2007. A phosphorylated form of Mel-18 targets the Ring1B histone H2A ubiquitin ligase to chromatin. Mol Cell 28, 107–120. [PubMed: 17936708]

Ema M, Takahashi S, Rossant J, 2006. Deletion of the selection cassette, but not cis-acting elements, in targeted Flk1-lacZ allele reveals Flk1 expression in multipotent mesodermal progenitors. Blood 107, 111–117. [PubMed: 16166582]

Endoh M, Endo TA, Endoh T, Fujimura Y, Ohara O, Toyoda T, Otte AP, Okano M, Brockdorff N, Vidal M, Koseki H, 2008. Polycomb group proteins Ring1A/B are functionally linked to the core transcriptional regulatory circuitry to maintain ES cell identity. Development 135, 1513–1524. [PubMed: 18339675]

Endoh M, Endo TA, Shinga J, Hayashi K, Farcas A, Ma KW, Ito S, Sharif J, Endoh T, Onaga N, Nakayama M, Ishikura T, Masui O, Kessler BM, Suda T, Ohara O, Okuda A, Klose R, Koseki H, 2017. PCGF6-PRC1 suppresses premature differentiation of mouse embryonic stem cells by regulating germ cell-related genes. Elife 6.

Engleka KA, Gitler AD, Zhang M, Zhou DD, High FA, Epstein JA, 2005. Insertion of Cre into the Pax3 locus creates a new allele of Splotch and identifies unexpected Pax3 derivatives. Dev Biol 280, 396–406. [PubMed: 15882581]

Engleka KA, Manderfield LJ, Brust RD, Li L, Cohen A, Dymecki SM, Epstein JA, 2012. Islet1 derivatives in the heart are of both neural crest and second heart field origin. Circ Res 110, 922–926. [PubMed: 22394517]

Farcas AM, Blackledge NP, Sudbery I, Long HK, McGouran JF, Rose NR, Lee S, Sims D, Cerase A, Sheahan TW, Koseki H, Brockdorff N, Ponting CP, Kessler BM, Klose RJ, 2012. KDM2B links the Polycomb Repressive Complex 1 (PRC1) to recognition of CpG islands. Elife 1, e00205. [PubMed: 23256043]

Feberwee HE, Feenstra I, Oberoi S, Sama IE, Ockeloen CW, Clum F, Slavotinek A, Kuijpers MA, Dooijes D, Kuijpers-Jagtman AM, Kleefstra T, Carels CE, 2014. Novel BCOR mutations in patients with oculofaciocardiodental (OFCD) syndrome. Clin Genet 85, 194–197. [PubMed: 23557072]

Frommer J, Margolies MR, 1971. Contribution of Meckel's cartilage to ossification of the mandible in mice. J Dent Res 50, 1260–1267. [PubMed: 5285785]

Gao Z, Zhang J, Bonasio R, Strino F, Sawai A, Parisi F, Kluger Y, Reinberg D, 2012. PCGF homologs, CBX proteins, and RYBP define functionally distinct PRC1 family complexes. Mol Cell 45, 344–356. [PubMed: 22325352]

Gearhart MD, Corcoran CM, Wamstad JA, Bardwell VJ, 2006. Polycomb group and SCF ubiquitin ligases are found in a novel BCOR complex that is recruited to BCL6 targets. Mol Cell Biol 26, 6880–6889. [PubMed: 16943429]

Ghetu AF, Corcoran CM, Cerchietti L, Bardwell VJ, Melnick A, Prive GG, 2008. Structure of a BCOR corepressor peptide in complex with the BCL6 BTB domain dimer. Mol Cell 29, 384–391. [PubMed: 18280243]

Gil J, O'Loghlen A, 2014. PRC1 complex diversity: where is it taking us? Trends Cell Biol 24, 632–641. [PubMed: 25065329]

Grossmann V, Tiacci E, Holmes AB, Kohlmann A, Martelli MP, Kern W, Spanhol-Rosseto A, Klein HU, Dugas M, Schindela S, Trifonov V, Schnittger S, Haferlach C, Bassan R, Wells VA, Spinelli O, Chan J, Rossi R, Baldoni S, De Carolis L, Goetze K, Serve H, Peceny R, Kreuzer KA, Oruzio D, Specchia G, Di Raimondo F, Fabbiano F, Sborgia M, Liso A, Farinelli L, Rambaldi A, Pasqualucci L, Rabadan R, Haferlach T, Falini B, 2011. Whole-exome sequencing identifies somatic mutations of BCOR in acute myeloid leukemia with normal karyotype. Blood 118, 6153–6163. [PubMed: 22012066]

Hadjantonakis AK, Cox LL, Tam PP, Nagy A, 2001. An X-linked GFP transgene reveals unexpected paternal X-chromosome activity in trophoblastic giant cells of the mouse placenta. Genesis 29, 133–140. [PubMed: 11252054]

Hamasaki T, Leingartner A, Ringstedt T, O'Leary DD, 2004. EMX2 regulates sizes and positioning of the primary sensory and motor areas in neocortex by direct specification of cortical progenitors. Neuron 43, 359–372. [PubMed: 15294144]

Hasso A, Casselman JW, Broadwell RA, 1995. Temporal bone congenital anomalies, in: Som PM, Curlin HD (Eds.), Head and neck imaging, 3rd ed. Mosby, St. Louis, USA, pp. 1351–1390.

Hatzi K, Jiang Y, Huang C, Garrett-Bakelman F, Gearhart MD, Giannopoulou EG, Zumbo P, Kirouac K, Bhaskara S, Polo JM, Kormaksson M, Mackerell AD Jr., Xue F, Mason CE, Hiebert SW, Prive GG, Cerchietti L, Bardwell VJ, Elemento O, Melnick A, 2013. A Hybrid Mechanism of Action for BCL6 in B Cells Defined by Formation of Functionally Distinct Complexes at Enhancers and Promoters. Cell Reports 4, 578–588. [PubMed: 23911289]

Hayashi S, Lewis P, Pevny L, McMahon AP, 2002. Efficient gene modulation in mouse epiblast using a Sox2Cre transgenic mouse strain. Mechanisms of development 119 Suppl 1, S97–S101. [PubMed: 14516668]

He J, Kallin EM, Tsukada Y, Zhang Y, 2008. The H3K36 demethylase Jhdm1b/Kdm2b regulates cell proliferation and senescence through p15(Ink4b). Nat Struct Mol Biol 15, 1169–1175. [PubMed: 18836456]

He J, Shen L, Wan M, Taranova O, Wu H, Zhang Y, 2013. Kdm2b maintains murine embryonic stem cell status by recruiting PRC1 complex to CpG islands of developmental genes. Nat Cell Biol 15, 373–384. [PubMed: 23502314]

Hedera P, Gorski JL, 2003. Oculo-facio-cardio-dental syndrome: skewed X chromosome inactivation in mother and daughter suggest X-linked dominant Inheritance. Am J Med Genet A 123A, 261–266. [PubMed: 14608648]

Hefti E, Trechsel U, Rufenacht H, Fleisch H, 1980. Use of dermestid beetles for cleaning bones. Calcif Tissue Int 31, 45–47. [PubMed: 6770972]

Hemberger MC, Pearsall RS, Zechner U, Orth A, Otto S, Ruschendorf F, Fundele R, Elliott R, 1999. Genetic dissection of X-linked interspecific hybrid placental dysplasia in congenic mouse strains. Genetics 153, 383–390. [PubMed: 10471720]

Herold T, Metzeler KH, Vosberg S, Hartmann L, Rollig C, Stolzel F, Schneider S, Hubmann M, Zellmeier E, Ksienzyk B, Jurinovic V, Pasalic Z, Kakadia PM, Dufour A, Graf A, Krebs S, Blum H, Sauerland MC, Buchner T, Berdel WE, Woermann BJ, Bornhauser M, Ehninger G, Mansmann U, Hiddemann W, Bohlander SK, Spiekermann K, Greif PA, 2014. Isolated trisomy 13 defines a genetically homogenous AML subgroup with high frequency of mutations in spliceosome genes and poor prognosis. Blood.

Hilton E, Black G, Bardwell VJ, 2008. The BCL-6 corepressor (BCOR) and Oculofaciocardiodental syndrome in: Epstein CJ, Erickson RP, Wynshaw-Boris AJ (Eds.), Inborn errors of development : the molecular basis of clinical disorders of morphogenesis, 2nd ed. Oxford University Press, Oxford; New York, pp. 987–994.

Hilton E, Johnston J, Whalen S, Okamoto N, Hatsukawa Y, Nishio J, Kohara H, Hirano Y, Mizuno S, Torii C, Kosaki K, Manouvrier S, Boute O, Perveen R, Law C, Moore A, Fitzpatrick D, Lemke J, Fellmann F, Debray FG, Dastot-Le-Moal F, Gerard M, Martin J, Bitoun P, Goossens M, Verloes A, Schinzel A, Bartholdi D, Bardakjian T, Hay B, Jenny K, Johnston K, Lyons M, Belmont JW, Biesecker LG, Giurgea I, Black G, 2009. BCOR analysis in patients with OFCD and Lenz microphthalmia syndromes, mental retardation with ocular anomalies, and cardiac laterality defects. Eur J Hum Genet 17, 1325–1335. [PubMed: 19367324]

Hilton EN, Manson FD, Urquhart JE, Johnston JJ, Slavotinek AM, Hedera P, Stattin EL, Nordgren A, Biesecker LG, Black GC, 2007. Left-sided embryonic expression of the BCL-6 corepressor, BCOR, is required for vertebrate laterality determination. Hum Mol Genet 16, 1773–1782. [PubMed: 17517692]

Ho AS, Ochoa A, Jayakumaran G, Zehir A, Valero Mayor C, Tepe J, Makarov V, Dalin MG, He J, Bailey M, Montesion M, Ross JS, Miller VA, Chan L, Ganly I, Dogan S, Katabi N, Tsipouras P, Ha P, Agrawal N, Solit DB, Futreal PA, El Naggar AK, Reis-Filho JS, Weigelt B, Ho AL,

Schultz N, Chan TA, Morris LG, 2019. Genetic hallmarks of recurrent/metastatic adenoid cystic carcinoma. J Clin Invest 129, 4276–4289. [PubMed: 31483290]

Horn D, Chyrek M, Kleier S, Luttgen S, Bolz H, Hinkel GK, Korenke GC, Riess A, Schell-Apacik C, Tinschert S, Wieczorek D, Gillessen-Kaesbach G, Kutsche K, 2005. Novel mutations in BCOR in three patients with oculo-facio-cardio-dental syndrome, but none in Lenz microphthalmia syndrome. Eur J Hum Genet 13, 563–569. [PubMed: 15770227]

Hsu WH, Chen CM, You LR, 2017. COUP-TFII is required for morphogenesis of the neural crest-derived tympanic ring. Sci Rep 7, 12386. [PubMed: 28959031]

Huang C, Hatzi K, Melnick A, 2013. Lineage-specific functions of Bcl-6 in immunity and inflammation are mediated by distinct biochemical mechanisms. Nat Immunol 14, 380–388. [PubMed: 23455674]

Huang X, Goudy SL, Ketova T, Litingtung Y, Chiang C, 2008. Gli3-deficient mice exhibit cleft palate associated with abnormal tongue development. Dev Dyn 237, 3079–3087. [PubMed: 18816854]

Huynh KD, Fischle W, Verdin E, Bardwell VJ, 2000. BCoR, a novel corepressor involved in BCL-6 repression. Genes Dev 14, 1810–1823. [PubMed: 10898795]

Jacques-Fricke BT, Roffers-Agarwal J, Gammill LS, 2012. DNA methyltransferase 3b is dispensable for mouse neural crest development. PLoS One 7, e47794. [PubMed: 23094090]

Jaskoll T, Zhou YM, Trump G, Melnick M, 2003. Ectodysplasin receptor-mediated signaling is essential for embryonic submandibular salivary gland development. Anat Rec A Discov Mol Cell Evol Biol 271, 322–331. [PubMed: 12629675]

Junco SE, Wang R, Gaipa JC, Taylor AB, Schirf V, Gearhart MD, Bardwell VJ, Demeler B, Hart PJ, Kim CA, 2013. Structure of the polycomb group protein PCGF1 in complex with BCOR reveals basis for binding selectivity of PCGF homologs. Structure 21, 665–671. [PubMed: 23523425]

Kaartinen V, Voncken JW, Shuler C, Warburton D, Bu D, Heisterkamp N, Groffen J, 1995. Abnormal lung development and cleft palate in mice lacking TGF-beta 3 indicates defects of epithelial-mesenchymal interaction. Nat Genet 11, 415–421. [PubMed: 7493022]

Keenan ID, Rhee HJ, Chaudhry B, Henderson DJ, 2012. Origin of non-cardiac endothelial cells from an Isl1+ lineage. FEBS Lett 586, 1790–1794. [PubMed: 22613570]

Kelly MJ, So J, Rogers AJ, Gregory G, Li J, Zethoven M, Gearhart MD, Bardwell VJ, Johnstone RW, Vervoort SJ, Kats LM, 2019. Bcor loss perturbs myeloid differentiation and promotes leukaemogenesis. Nat Commun 10, 1347. [PubMed: 30902969]

Kerppola TK, 2009. Polycomb group complexes--many combinations, many functions. Trends Cell Biol 19, 692–704. [PubMed: 19889541]

Komuro I, Izumo S, 1993. Csx: a murine homeobox-containing gene specifically expressed in the developing heart. Proc Natl Acad Sci U S A 90, 8145–8149. [PubMed: 7690144]

Kondo Y, Saitsu H, Miyamoto T, Nishiyama K, Tsurusaki Y, Doi H, Miyake N, Ryoo NK, Kim JH, Yu YS, Matsumoto N, 2012. A family of oculofaciocardiodental syndrome (OFCD) with a novel BCOR mutation and genomic rearrangements involving NHS. J Hum Genet 57, 197–201. [PubMed: 22301464]

Kotov JA, Kotov DI, Linehan JL, Bardwell VJ, Gearhart MD, Jenkins MK, 2019. BCL6 corepressor contributes to Th17 cell formation by inhibiting Th17 fate suppressors. J Exp Med 216, 1450–1464. [PubMed: 31053612]

Kutscher LM, Okonechnikov K, Batora NV, Clark J, Silva PBG, Vouri M, van Rijn S, Sieber L, Statz B, Gearhart MD, Shiraishi R, Mack N, Orr BA, Korshunov A, Gudenas BL, Smith KS, Mercier AL, Ayrault O, Hoshino M, Kool M, von Hoff K, Graf N, Fleischhack G, Bardwell VJ, Pfister SM, Northcott PA, Kawauchi D, 2020. Functional loss of a noncanonical BCOR-PRC1.1 complex accelerates SHH-driven medulloblastoma formation. Genes Dev. 34,1161–1176. [PubMed: 32820036]

Lang D, Lu MM, Huang L, Engleka KA, Zhang M, Chu EY, Lipner S, Skoultchi A, Millar SE, Epstein JA, 2005. Pax3 functions at a nodal point in melanocyte stem cell differentiation. Nature 433, 884–887. [PubMed: 15729346]

Lavrin IO, McLean W, Seegmiller RE, Olsen BR, Hay ED, 2001. The mechanism of palatal clefting in the Col11a1 mutant mouse. Arch Oral Biol 46, 865–869. [PubMed: 11420059]

Laws N, Hoey A, 2004. Progression of kyphosis in mdx mice. J Appl Physiol (1985) 97, 1970–1977. [PubMed: 15234960]

Le Y, Miller JL, Sauer B, 1999. GFPcre fusion vectors with enhanced expression. Anal Biochem 270, 334–336. [PubMed: 10334853]

Levine SS, Weiss A, Erdjument-Bromage H, Shao Z, Tempst P, Kingston RE, 2002. The core of the polycomb repressive complex is compositionally and functionally conserved in flies and humans. Molecular and cellular biology 22, 6070–6078. [PubMed: 12167701]

Lewandoski M, Meyers EN, Martin GR, 1997. Analysis of Fgf8 gene function in vertebrate development. Cold Spring Harb Symp Quant Biol 62, 159–168. [PubMed: 9598348]

Li F, Fu G, Liu Y, Miao X, Li Y, Yang X, Zhang X, Yu D, Gan L, Qiu M, Chen Y, Zhang Z, Zhang Z, 2017. ISLET1-Dependent beta-Catenin/Hedgehog Signaling Is Required for Outgrowth of the Lower Jaw. Mol Cell Biol 37.

Li Y, Sabari BR, Panchenko T, Wen H, Zhao D, Guan H, Wan L, Huang H, Tang Z, Zhao Y, Roeder RG, Shi X, Allis CD, Li H, 2016. Molecular Coupling of Histone Crotonylation and Active Transcription by AF9 YEATS Domain. Mol Cell 62, 181–193. [PubMed: 27105114]

Liu P, Jenkins NA, Copeland NG, 2003. A highly efficient recombineering-based method for generating conditional knockout mutations. Genome Res 13, 476–484. [PubMed: 12618378]

Lozic B, Ljubkovic J, Panduric DG, Saltvig I, Kutsche K, Krzelj V, Zemunik T, 2012. Oculo-facio-cardio-dental syndrome in three succeeding generations: genotypic data and phenotypic features. Braz J Med Biol Res 45, 1315–1319. [PubMed: 22983184]

Luis NM, Morey L, Di Croce L, Benitah SA, 2012. Polycomb in stem cells: PRC1 branches out. Cell Stem Cell 11, 16–21. [PubMed: 22770239]

Lyon MF, 1961. Gene action in the X-chromosome of the mouse (Mus musculus L.). Nature 190, 372–373. [PubMed: 13764598]

Ma AS, Grigg JR, Ho G, Prokudin I, Farnsworth E, Holman K, Cheng A, Billson FA, Martin F, Fraser C, Mowat D, Smith J, Christodoulou J, Flaherty M, Bennetts B, Jamieson RV, 2016. Sporadic and Familial Congenital Cataracts: Mutational Spectrum and New Diagnoses Using Next-Generation Sequencing. Hum Mutat 37, 371–384. [PubMed: 26694549]

Ma Q, Zhou B, Pu WT, 2008. Reassessment of Isl1 and Nkx2–5 cardiac fate maps using a Gata4-based reporter of Cre activity. Dev Biol 323, 98–104. [PubMed: 18775691]

Madisen L, Zwingman TA, Sunkin SM, Oh SW, Zariwala HA, Gu H, Ng LL, Palmiter RD, Hawrylycz MJ, Jones AR, Lein ES, Zeng H, 2010. A robust and high-throughput Cre reporting and characterization system for the whole mouse brain. Nat Neurosci 13, 133–140. [PubMed: 20023653]

Mallo M, 2018. Reassessing the Role of Hox Genes during Vertebrate Development and Evolution. Trends Genet 34, 209–217. [PubMed: 29269261]

Mansouri A, Yokota Y, Wehr R, Copeland NG, Jenkins NA, Gruss P, 1997. Paired-related murine homeobox gene expressed in the developing sclerotome, kidney, and nervous system. Dev Dyn 210, 53–65. [PubMed: 9286595]

Marashi AH, Gorlin RJ, 1990. Radiculomegaly of canines and congenital cataracts--a syndrome? Oral Surg Oral Med Oral Pathol 70, 802–803. [PubMed: 2263345]

McFadden DG, Barbosa AC, Richardson JA, Schneider MD, Srivastava D, Olson EN, 2005. The Hand1 and Hand2 transcription factors regulate expansion of the embryonic cardiac ventricles in a gene dosage-dependent manner. Development 132, 189–201. [PubMed: 15576406]

McGovern E, Al-Mudaffer M, McMahon C, Brosnahan D, Fleming P, Reardon W, 2006. Oculo-facio-cardio-dental syndrome in a mother and daughter. Int J Oral Maxillofac Surg 35, 1060–1062. [PubMed: 16829040]

Metzler MA, Raja S, Elliott KH, Friedl RM, Tran NQH, Brugmann SA, Larsen M, Sandell LL, 2018. RDH10-mediated retinol metabolism and RARalpha-mediated retinoic acid signaling are required for submandibular salivary gland initiation. Development 145.

Moreira de Mello JC, de Araujo ES, Stabellini R, Fraga AM, de Souza JE, Sumita DR, Camargo AA, Pereira LV, 2010. Random X inactivation and extensive mosaicism in human placenta revealed by analysis of allele-specific gene expression along the X chromosome. PLoS One 5, e10947. [PubMed: 20532033]

Morris LGT, Chandramohan R, West L, Zehir A, Chakravarty D, Pfister DG, Wong RJ, Lee NY, Sherman EJ, Baxi SS, Ganly I, Singh B, Shah JP, Shaha AR, Boyle JO, Patel SG, Roman BR, Barker CA, McBride SM, Chan TA, Dogan S, Hyman DM, Berger MF, Solit DB, Riaz N, Ho AL, 2017. The Molecular Landscape of Recurrent and Metastatic Head and Neck Cancers: Insights From a Precision Oncology Sequencing Platform. JAMA Oncol 3, 244–255. [PubMed: 27442865]

Moses KA, DeMayo F, Braun RM, Reecy JL, Schwartz RJ, 2001. Embryonic expression of an Nkx2–5/Cre gene using ROSA26 reporter mice. Genesis 31, 176–180. [PubMed: 11783008]

Nakagawa Y, O'Leary DD, 2003. Dynamic patterned expression of orphan nuclear receptor genes RORalpha and RORbeta in developing mouse forebrain. Dev Neurosci 25, 234–244. [PubMed: 12966220]

Ng D, Thakker N, Corcoran CM, Donnai D, Perveen R, Schneider A, Hadley DW, Tifft C, Zhang L, Wilkie AO, van der Smagt JJ, Gorlin RJ, Burgess SM, Bardwell VJ, Black GC, Biesecker LG, 2004. Oculofaciocardiodental and Lenz microphthalmia syndromes result from distinct classes of mutations in BCOR. Nat Genet 36, 411–416. [PubMed: 15004558]

Nicholas FW, 2003. Online Mendelian Inheritance in Animals (OMIA): a comparative knowledgebase of genetic disorders and other familial traits in non-laboratory animals. Nucleic Acids Res 31, 275–277. [PubMed: 12520001]

O'Byrne JJ, Laffan E, Murray DJ, Reardon W, 2017. Oculo-facio-cardio-dental syndrome with craniosynostosis, temporal hypertrichosis, and deafness. Am J Med Genet A 173, 1374–1377. [PubMed: 28317252]

Obwegeser HL, Gorlin RJ, 1997. Oculo-facio-cardio-dental (OFCD) syndrome. Clin Dysmorphol 6, 281–283. [PubMed: 9220201]

Ogawa H, Ishiguro K, Gaubatz S, Livingston DM, Nakatani Y, 2002. A complex with chromatin modifiers that occupies E2F- and Myc-responsive genes in G0 cells. Science 296, 1132–1136. [PubMed: 12004135]

Parada C, Chai Y, 2015. Mandible and Tongue Development. Curr Top Dev Biol 115, 31–58. [PubMed: 26589920]

Perez-Garcia V, Fineberg E, Wilson R, Murray A, Mazzeo CI, Tudor C, Sienerth A, White JK, Tuck E, Ryder EJ, Gleeson D, Siragher E, Wardle-Jones H, Staudt N, Wali N, Collins J, Geyer S, Busch-Nentwich EM, Galli A, Smith JC, Robertson E, Adams DJ, Weninger WJ, Mohun T, Hemberger M, 2018. Placentation defects are highly prevalent in embryonic lethal mouse mutants. Nature 555, 463–468. [PubMed: 29539633]

Perez-Gomez R, Haro E, Fernandez-Guerrero M, Bastida MF, Ros MA, 2018. Role of Hox genes in regulating digit patterning. Int J Dev Biol 62, 797–805. [PubMed: 30604849]

Pfaff SL, Mendelsohn M, Stewart CL, Edlund T, Jessell TM, 1996. Requirement for LIM homeobox gene Isl1 in motor neuron generation reveals a motor neuron-dependent step in interneuron differentiation. Cell 84, 309–320. [PubMed: 8565076]

Pierron G, Tirode F, Lucchesi C, Reynaud S, Ballet S, Cohen-Gogo S, Perrin V, Coindre JM, Delattre O, 2012. A new subtype of bone sarcoma defined by BCOR-CCNB3 gene fusion. Nat Genet 44, 461–466. [PubMed: 22387997]

Prall OW, Menon MK, Solloway MJ, Watanabe Y, Zaffran S, Bajolle F, Biben C, McBride JJ, Robertson BR, Chaulet H, Stennard FA, Wise N, Schaft D, Wolstein O, Furtado MB, Shiratori H, Chien KR, Hamada H, Black BL, Saga Y, Robertson EJ, Buckingham ME, Harvey RP, 2007. An Nkx2–5/Bmp2/Smad1 negative feedback loop controls heart progenitor specification and proliferation. Cell 128, 947–959. [PubMed: 17350578]

Pugh TJ, Weeraratne SD, Archer TC, Pomeranz Krummel DA, Auclair D, Bochicchio J, Carneiro MO, Carter SL, Cibulskis K, Erlich RL, Greulich H, Lawrence MS, Lennon NJ, McKenna A, Meldrim J, Ramos AH, Ross MG, Russ C, Shefler E, Sivachenko A, Sogoloff B, Stojanov P, Tamayo P, Mesirov JP, Amani V, Teider N, Sengupta S, Francois JP, Northcott PA, Taylor MD, Yu F, Crabtree GR, Kautzman AG, Gabriel SB, Getz G, Jager N, Jones DT, Lichter P, Pfister SM, Roberts TM, Meyerson M, Pomeroy SL, Cho YJ, 2012. Medulloblastoma exome sequencing uncovers subtype-specific somatic mutations. Nature 488, 106–110. [PubMed: 22820256]

Ragge N, Isidor B, Bitoun P, Odent S, Giurgea I, Cogne B, Deb W, Vincent M, Le Gall J, Morton J, Lim D, Study DDD, Le Meur G, Zazo Seco C, Zafeiropoulou D, Bax D, Zwijnenburg P, Arteche

A, Swafiri ST, Cleaver R, McEntagart M, Kini U, Newman W, Ayuso C, Corton M, Herenger Y, Jeanne M, Calvas P, Chassaing N, 2018. Expanding the phenotype of the X-linked BCOR microphthalmia syndromes. Hum Genet.

Ramaesh T, Bard JB, 2003. The growth and morphogenesis of the early mouse mandible: a quantitative analysis. J Anat 203, 213–222. [PubMed: 12924821]

Richany SF, Bast TH, Anson BJ, 1956. The development of the first branchial arch in man and the fate of Meckel's cartilage. Q Bull Northwest Univ Med Sch 30, 331–355. [PubMed: 13408429]

Rodriguez CI, Buchholz F, Galloway J, Sequerra R, Kasper J, Ayala R, Stewart AF, Dymecki SM, 2000. High-efficiency deleter mice show that FLPe is an alternative to Cre-loxP. Nat Genet 25, 139–140. [PubMed: 10835623]

Roy A, Kumar V, Zorman B, Fang E, Haines KM, Doddapaneni H, Hampton OA, White S, Bavle AA, Patel NR, Eldin KW, John Hicks M, Rakheja D, Leavey PJ, Skapek SX, Amatruda JF, Nuchtern JG, Chintagumpala MM, Wheeler DA, Plon SE, Sumazin P, Parsons DW, 2015. Recurrent internal tandem duplications of BCOR in clear cell sarcoma of the kidney. Nat Commun 6, 8891. [PubMed: 26573325]

Sakano D, Kato A, Parikh N, McKnight K, Terry D, Stefanovic B, Kato Y, 2010. BCL6 canalizes Notch-dependent transcription, excluding Mastermind-like1 from selected target genes during left-right patterning. Dev Cell 18, 450–462. [PubMed: 20230751]

Sanchez C, Sanchez I, Demmers JA, Rodriguez P, Strouboulis J, Vidal M, 2007. Proteomics analysis of Ring1B/Rnf2 interactors identifies a novel complex with the Fbxl10/Jhdm1B histone demethylase and the Bcl6 interacting corepressor. Mol Cell Proteomics 6, 820–834. [PubMed: 17296600]

Schuettengruber B, Bourbon HM, Di Croce L, Cavalli G, 2017. Genome Regulation by Polycomb and Trithorax: 70 Years and Counting. Cell 171, 34–57. [PubMed: 28938122]

Seki M, Nishimura R, Yoshida K, Shimamura T, Shiraishi Y, Sato Y, Kato M, Chiba K, Tanaka H, Hoshino N, Nagae G, Shiozawa Y, Okuno Y, Hosoi H, Tanaka Y, Okita H, Miyachi M, Souzaki R, Taguchi T, Koh K, Hanada R, Kato K, Nomura Y, Akiyama M, Oka A, Igarashi T, Miyano S, Aburatani H, Hayashi Y, Ogawa S, Takita J, 2015. Integrated genetic and epigenetic analysis defines novel molecular subgroups in rhabdomyosarcoma. Nat Commun 6, 7557. [PubMed: 26138366]

Shimamura K, Hartigan DJ, Martinez S, Puelles L, Rubenstein JL, 1995. Longitudinal organization of the anterior neural plate and neural tube. Development 121, 3923–3933. [PubMed: 8575293]

Shirai M, Osugi T, Koga H, Kaji Y, Takimoto E, Komuro I, Hara J, Miwa T, Yamauchi-Takihara K, Takihara Y, 2002. The Polycomb-group gene Rae28 sustains Nkx2.5/Csx expression and is essential for cardiac morphogenesis. J Clin Invest 110, 177–184. [PubMed: 12122109]

Simon JA, Kingston RE, 2013. Occupying chromatin: Polycomb mechanisms for getting to genomic targets, stopping transcriptional traffic, and staying put. Mol Cell 49, 808–824. [PubMed: 23473600]

Specht K, Zhang L, Sung YS, Nucci M, Dry S, Vaiyapuri S, Richter GH, Fletcher CD, Antonescu CR, 2016. Novel BCOR-MAML3 and ZC3H7B-BCOR Gene Fusions in Undifferentiated Small Blue Round Cell Sarcomas. Am J Surg Pathol 40, 433–442. [PubMed: 26752546]

Srinivas S, Watanabe T, Lin CS, William CM, Tanabe Y, Jessell TM, Costantini F, 2001. Cre reporter strains produced by targeted insertion of EYFP and ECFP into the ROSA26 locus. BMC Dev Biol 1, 4. [PubMed: 11299042]

Srinivasan RS, de Erkenez AC, Hemenway CS, 2003. The mixed lineage leukemia fusion partner AF9 binds specific isoforms of the BCL-6 corepressor. Oncogene 22, 3395–3406. [PubMed: 12776190]

Stanley EG, Biben C, Elefanty A, Barnett L, Koentgen F, Robb L, Harvey RP, 2002. Efficient Cre-mediated deletion in cardiac progenitor cells conferred by a 3'UTR-ires-Cre allele of the homeobox gene Nkx2–5. Int J Dev Biol 46, 431–439. [PubMed: 12141429]

Storm EE, Garel S, Borello U, Hebert JM, Martinez S, McConnell SK, Martin GR, Rubenstein JL, 2006. Dose-dependent functions of Fgf8 in regulating telencephalic patterning centers. Development 133, 1831–1844. [PubMed: 16613831]

Sujatha RS, Namita R, 2008. Oculofaciocardiodental syndrome: report of a rare case. Quintessence Int 39, 821–825. [PubMed: 19093058]

Sun Y, Liang X, Najafi N, Cass M, Lin L, Cai CL, Chen J, Evans SM, 2007. Islet 1 is expressed in distinct cardiovascular lineages, including pacemaker and coronary vascular cells. Dev Biol 304, 286–296. [PubMed: 17258700]

Surapornsawasd T, Ogawa T, Tsuji M, Moriyama K, 2014. Oculofaciocardiodental syndrome: novel BCOR mutations and expression in dental cells. J Hum Genet 59, 314–320. [PubMed: 24694763]

Suzumori N, Kaname T, Muramatsu Y, Yanagi K, Kumagai K, Mizuno S, Naritomi K, Saitoh S, Sugiura-Ogasawara M, 2013. Prenatal diagnosis of X-linked recessive Lenz microphthalmia syndrome. J Obstet Gynaecol Res.

Takagi N, Sasaki M, 1975. Preferential inactivation of the paternally derived X chromosome in the extraembryonic membranes of the mouse. Nature 256, 640–642. [PubMed: 1152998]

Takihara Y, Tomotsune D, Shirai M, Katoh-Fukui Y, Nishii K, Motaleb MA, Nomura M, Tsuchiya R, Fujita Y, Shibata Y, Higashinakagawa T, Shimada K, 1997. Targeted disruption of the mouse homologue of the Drosophila polyhomeotic gene leads to altered anteroposterior patterning and neural crest defects. Development 124, 3673–3682. [PubMed: 9367423]

Tan SS, Williams EA, Tam PP, 1993. X-chromosome inactivation occurs at different times in different tissues of the post-implantation mouse embryo. Nat Genet 3, 170–174. [PubMed: 8499950]

Tanaka K, Kato A, Angelocci C, Watanabe M, Kato Y, 2014. A potential molecular pathogenesis of cardiac/laterality defects in Oculo-Facio-Cardio-Dental syndrome. Dev Biol 387, 28–36. [PubMed: 24440151]

Tanaka T, Nakajima-Takagi Y, Aoyama K, Tara S, Oshima M, Saraya A, Koide S, Si S, Manabe I, Sanada M, Nakayama M, Masuko M, Sone H, Koseki H, Iwama A, 2017. Internal deletion of BCOR reveals a tumor suppressor function for BCOR in T lymphocyte malignancies. J Exp Med 214, 2901–2913. [PubMed: 28827447]

Tao W, Lai E, 1992. Telencephalon-restricted expression of BF-1, a new member of the HNF-3/fork head gene family, in the developing rat brain. Neuron 8, 957–966. [PubMed: 1350202]

Tara S, Isshiki Y, Nakajima-Takagi Y, Oshima M, Aoyama K, Tanaka T, Shinoda D, Koide S, Saraya A, Miyagi S, Manabe I, Matsui H, Koseki H, Bardwell VJ, Iwama A, 2018. Bcor insufficiency promotes initiation and progression of myelodysplastic syndrome. Blood 132, 2470–2483. [PubMed: 30228234]

Trojer P, Cao AR, Gao Z, Li Y, Zhang J, Xu X, Li G, Losson R, Erdjument-Bromage H, Tempst P, Farnham PJ, Reinberg D, 2011. L3MBTL2 protein acts in concert with PcG protein-mediated monoubiquitination of H2A to establish a repressive chromatin structure. Mol Cell 42, 438–450. [PubMed: 21596310]

Turgeon B, Meloche S, 2009. Interpreting neonatal lethal phenotypes in mouse mutants: insights into gene function and human diseases. Physiol Rev 89, 1–26. [PubMed: 19126753]

Ueno-Yokohata H, Okita H, Nakasato K, Akimoto S, Hata J, Koshinaga T, Fukuzawa M, Kiyokawa N, 2015. Consistent in-frame internal tandem duplications of BCOR characterize clear cell sarcoma of the kidney. Nat Genet 47, 861–863. [PubMed: 26098867]

Vialli M, 1951. [Use of Alcian blue 8 G S in the study of mucopolysaccharides]. Boll Soc Ital Biol Sper 27, 597–599. [PubMed: 14869481]

Vidal M, Starowicz K, 2017. Polycomb complexes PRC1 and their function in hematopoiesis. Exp Hematol 48, 12–31. [PubMed: 28087428]

Voncken JW, Roelen BA, Roefs M, de Vries S, Verhoeven E, Marino S, Deschamps J, van Lohuizen M, 2003. Rnf2 (Ring1b) deficiency causes gastrulation arrest and cell cycle inhibition. Proc Natl Acad Sci U S A 100, 2468–2473. [PubMed: 12589020]

Wamstad JA, Bardwell VJ, 2007. Characterization of Bcor expression in mouse development. Gene Expr Patterns 7, 550–557. [PubMed: 17344103]

Wamstad JA, Corcoran CM, Keating AM, Bardwell VJ, 2008. Role of the transcriptional corepressor Bcor in embryonic stem cell differentiation and early embryonic development. PLoS One 3, e2814. [PubMed: 18795143]

Wang H, Wang L, Erdjument-Bromage H, Vidal M, Tempst P, Jones RS, Zhang Y, 2004. Role of histone H2A ubiquitination in Polycomb silencing. Nature 431, 873–878. [PubMed: 15386022]

Wang Z, Gearhart MD, Lee YW, Kumar I, Ramazanov B, Zhang Y, Hernandez C, Lu AY, Neuenkirchen N, Deng J, Jin J, Kluger Y, Neubert TA, Bardwell VJ, Ivanova NB, 2018. A Non-canonical BCOR-PRC1.1 Complex Represses Differentiation Programs in Human ESCs. Cell Stem Cell 22, 235–251 e239. [PubMed: 29337181]

West JD, Frels WI, Chapman VM, Papaioannou VE, 1977. Preferential expression of the maternally derived X chromosome in the mouse yolk sac. Cell 12, 873–882. [PubMed: 597862]

Wilkie AO, Taylor D, Scambler PJ, Baraitser M, 1993. Congenital cataract, microphthalmia and septal heart defect in two generations: a new syndrome? Clin Dysmorphol 2, 114–119. [PubMed: 8281271]

Wu H, Luo J, Yu H, Rattner A, Mo A, Wang Y, Smallwood PM, Erlanger B, Wheelan SJ, Nathans J, 2014. Cellular resolution maps of x chromosome inactivation: implications for neural development, function, and disease. Neuron 81, 103–119. [PubMed: 24411735]

Wu X, Gong Y, Yue J, Qiang B, Yuan J, Peng X, 2008. Cooperation between EZH2, NSPc1-mediated histone H2A ubiquitination and Dnmt1 in HOX gene silencing. Nucleic Acids Res 36, 3590–3599. [PubMed: 18460542]

Wu X, Johansen JV, Helin K, 2013. Fbxl10/Kdm2b recruits polycomb repressive complex 1 to CpG islands and regulates H2A ubiquitylation. Mol Cell 49, 1134–1146. [PubMed: 23395003]

Yamamoto Y, Abe A, Emi N, 2014. Clarifying the impact of polycomb complex component disruption in human cancers. Mol Cancer Res 12, 479–484. [PubMed: 24515802]

Yan L, Ping N, Zhu M, Sun A, Xue Y, Ruan C, Drexler HG, Macleod RA, Wu D, Chen S, 2012. Clinical, immunophenotypic, cytogenetic, and molecular genetic features in 117 adult patients with mixed-phenotype acute leukemia defined by WHO-2008 classification. Haematologica.

Yang JA, Tubo NJ, Gearhart MD, Bardwell VJ, Jenkins MK, 2015. Cutting edge: Bcl6-interacting corepressor contributes to germinal center T follicular helper cell formation and B cell helper function. J Immunol 194, 5604–5608. [PubMed: 25964495]

Yang L, Cai CL, Lin L, Qyang Y, Chung C, Monteiro RM, Mummery CL, Fishman GI, Cogen A, Evans S, 2006. Isl1Cre reveals a common Bmp pathway in heart and limb development. Development 133, 1575–1585. [PubMed: 16556916]

Yoshida K, Sanada M, Shiraishi Y, Nowak D, Nagata Y, Yamamoto R, Sato Y, Sato-Otsubo A, Kon A, Nagasaki M, Chalkidis G, Suzuki Y, Shiosaka M, Kawahata R, Yamaguchi T, Otsu M, Obara N, Sakata-Yanagimoto M, Ishiyama K, Mori H, Nolte F, Hofmann WK, Miyawaki S, Sugano S, Haferlach C, Koeffler HP, Shih LY, Haferlach T, Chiba S, Nakauchi H, Miyano S, Ogawa S, 2011. Frequent pathway mutations of splicing machinery in myelodysplasia. Nature 478, 64–69. [PubMed: 21909114]

Yoshida Y, Nobusawa S, Nakata S, Nakada M, Arakawa Y, Mineharu Y, Sugita Y, Yoshioka T, Araki A, Sato Y, Takeshima H, Okada M, Nishi A, Yamazaki T, Kohashi K, Oda Y, Hirato J, Yokoo H, 2018. CNS high-grade neuroepithelial tumor with BCOR internal tandem duplication: a comparison with its counterparts in the kidney and soft tissue. Brain Pathol 28, 710–720. [PubMed: 29226988]

Yu K, Ornitz DM, 2011. Histomorphological study of palatal shelf elevation during murine secondary palate formation. Dev Dyn 240, 1737–1744. [PubMed: 21618642]

Zhang J, Benavente CA, McEvoy J, Flores-Otero J, Ding L, Chen X, Ulyanov A, Wu G, Wilson M, Wang J, Brennan R, Rusch M, Manning AL, Ma J, Easton J, Shurtleff S, Mullighan C, Pounds S, Mukatira S, Gupta P, Neale G, Zhao D, Lu C, Fulton RS, Fulton LL, Hong X, Dooling DJ, Ochoa K, Naeve C, Dyson NJ, Mardis ER, Bahrami A, Ellison D, Wilson RK, Downing JR, Dyer MA, 2012. A novel retinoblastoma therapy from genomic and epigenetic analyses. Nature 481, 329–334. [PubMed: 22237022]

Zhou Y, Wojcik A, Sanders VR, Rahmani B, Kurup SP, 2017. Ocular findings in a patient with oculofaciocardiodental (OFCD) syndrome and a novel BCOR pathogenic variant. Int Ophthalmol.

Zhu G, Fei T, Li Z, Yan X, Chen YG, 2015a. Activin Regulates Self-renewal and Differentiation of Trophoblast Stem Cells by Down-regulating the X Chromosome Gene Bcor. J Biol Chem 290, 22019–22029. [PubMed: 26221038]

Zhu X, Dai FR, Wang J, Zhang Y, Tan ZP, Zhang Y, 2015b. Novel BCOR mutation in a boy with Lenz microphthalmia/oculo-facio-cardio-dental (OFCD) syndrome. Gene 571, 142–144. [PubMed: 26196063]

Zhuang S, Zhang Q, Zhuang T, Evans SM, Liang X, Sun Y, 2013. Expression of Isl1 during mouse development. Gene Expr Patterns 13, 407–412. [PubMed: 23906961]

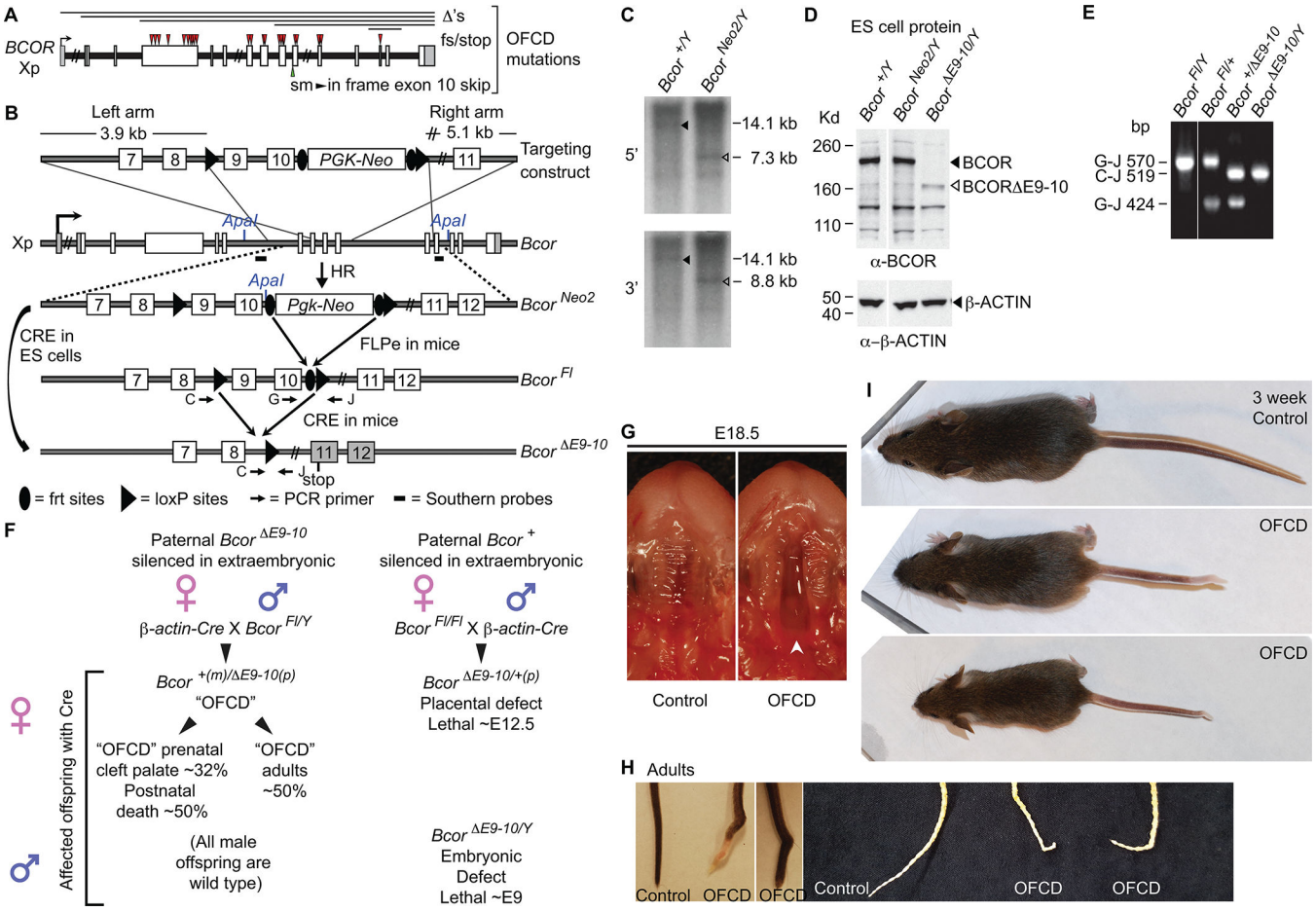

Figure 1: Generation of conditional *Bcor* allele.

(A) Diagram of human *BCOR* locus showing position of OFCD deletions (Δ) and mutations that generate frame shifts (fs) or stop codons (red triangles), and a splice site mutation (sm) leading to an in-frame exon 10 deletion (green triangle). (Note: splice site mutation sequence is shown in Figure 1d of (Ng et al., 2004). This mutation corresponds to family OFCD1 with IVS9G->T mutation (not IVS8G->T as stated), while family OFCD2 is actually IVS10G->A; L. Biesecker pers. comm.). (B) Diagram of *Bcor* gene targeting strategy. Homologous recombination in embryonic stem (ES) cells generated the *Bcor* ^{Neo2} allele, in which exons 9 and 10 of *Bcor* are flanked by loxP sites. Immediately downstream of exon 10, *Bcor* ^{Neo2} also contains a neomycin resistance cassette (Pgk-Em7-*Neo-bGH1pA*, shortened to *Pgk-Neo*) flanked by recognition sites for the FLP recombinase (frt sites), allowing its excision. *Bcor* ^{Fl} allele was generated by deleting *Pgk-Neo* cassette in mice expressing FLPe. CRE-mediated recombination excises exons 9 and 10, generating a premature stop codon in the now out-of-frame exon 11. Genotyping PCR primers and Southern probes are indicated. (C) Southern blot hybridization of the wild type and targeted ES cell genomic DNA, digested with *Apa*I, reveals successful homologous recombination of both the 3' and 5' homology arms. The *Apa*I site introduced immediately upstream of the 5' frt site in the targeting vector results in a 7.3 kb band recognized by the 5' probe and an 8.8 kb band recognized by the 3' probe. (D) Western blot analysis of wild-type, *Bcor* ^{Neo2},

and *Bcor* $^{\Delta E9-10/Y}$ ES cell protein extracts shows that the targeted *Bcor* ^{Neo2} cells display wild-type levels of full length BCOR and the *Bcor* $^{\Delta E9-10/Y}$ cells lack full-length BCOR and contain reduced amounts of a C-terminally truncated version of BCOR (BCORΔE9–10), which is unable to interact with KDM2B, PCGF1/3, and other PRC1 proteins and is thus predicted to be non-functional. ß-ACTIN levels were used as a loading control (bottom panel). (E) Multiplex PCR genotyping reaction of genomic DNA, using primers C, G and J, identifies all three alleles: wild type (424 bp), *Bcor* ^{Fl} (570 bp), and *Bcor* $^{\Delta E9-10}$ (519 bp). (F) Breeding strategies with *β-actin-Cre* and summary of outcomes. (G) E18.5 gross morphology of the maxillary region (mandibles removed) highlighting cleft palate (arrowhead) in OFCD but not control animal. Representative images of control and OFCD mice showing (H) kinked tails in adults and adult skeletal preparations, and (I) size at weaning.

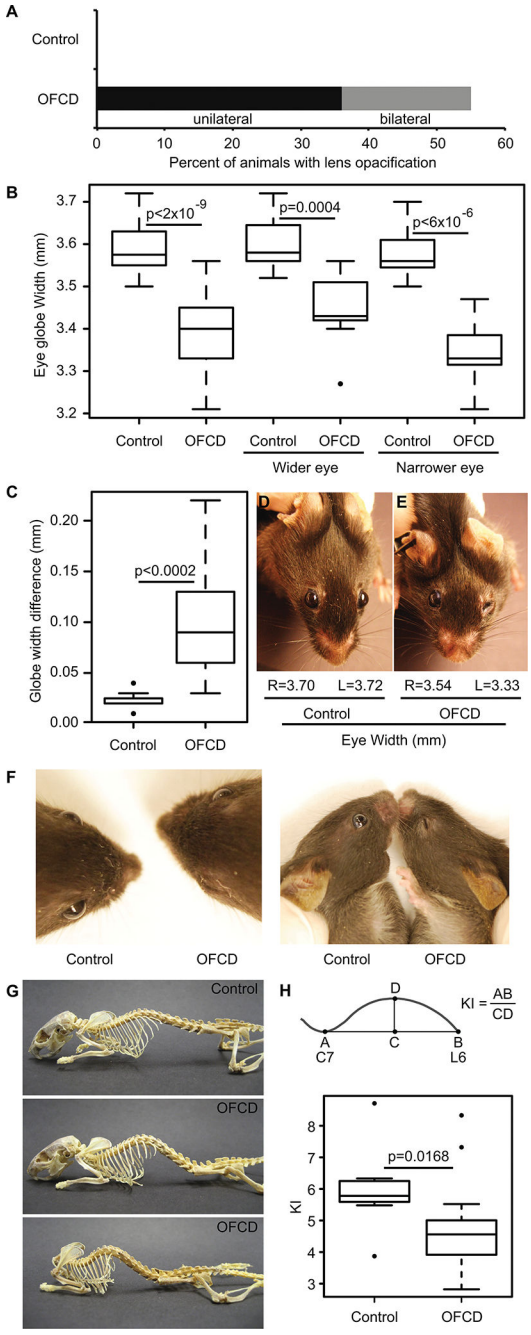

Figure 2. Ocular defects and kyphosis in OFCD mice.

(A) Bar plot of lens opacification in animals ages 3–28 weeks. (B) Boxplots of eye globe widths including all globes or separated by wider and narrower eye in each animal. (C) Boxplots of the eye globe width differences within each animal. (D-F) Images of paired littermate adult control and OFCD heads, note visible lens opacification in E and ptosis in E and F. Dorsal (left panel) and lateral (right panel) views of the same animals are shown in F. (G) Images of dermestid skeletal preparations of adult control and OFCD animals. Note kyphosis in OFCD skeletons. (H) Kyphosis index (KI) in control and OFCD animals. Distance AB is from the posterior edge of vertebrae C7 to the posterior edge of L6. CD is

the distance from line AB to the dorsal border of the vertebral body farthest from that line (Laws and Hoey, 2004). p values are from one-sided *t* tests for B and H and Welsh one-sided *t*-tests for C.

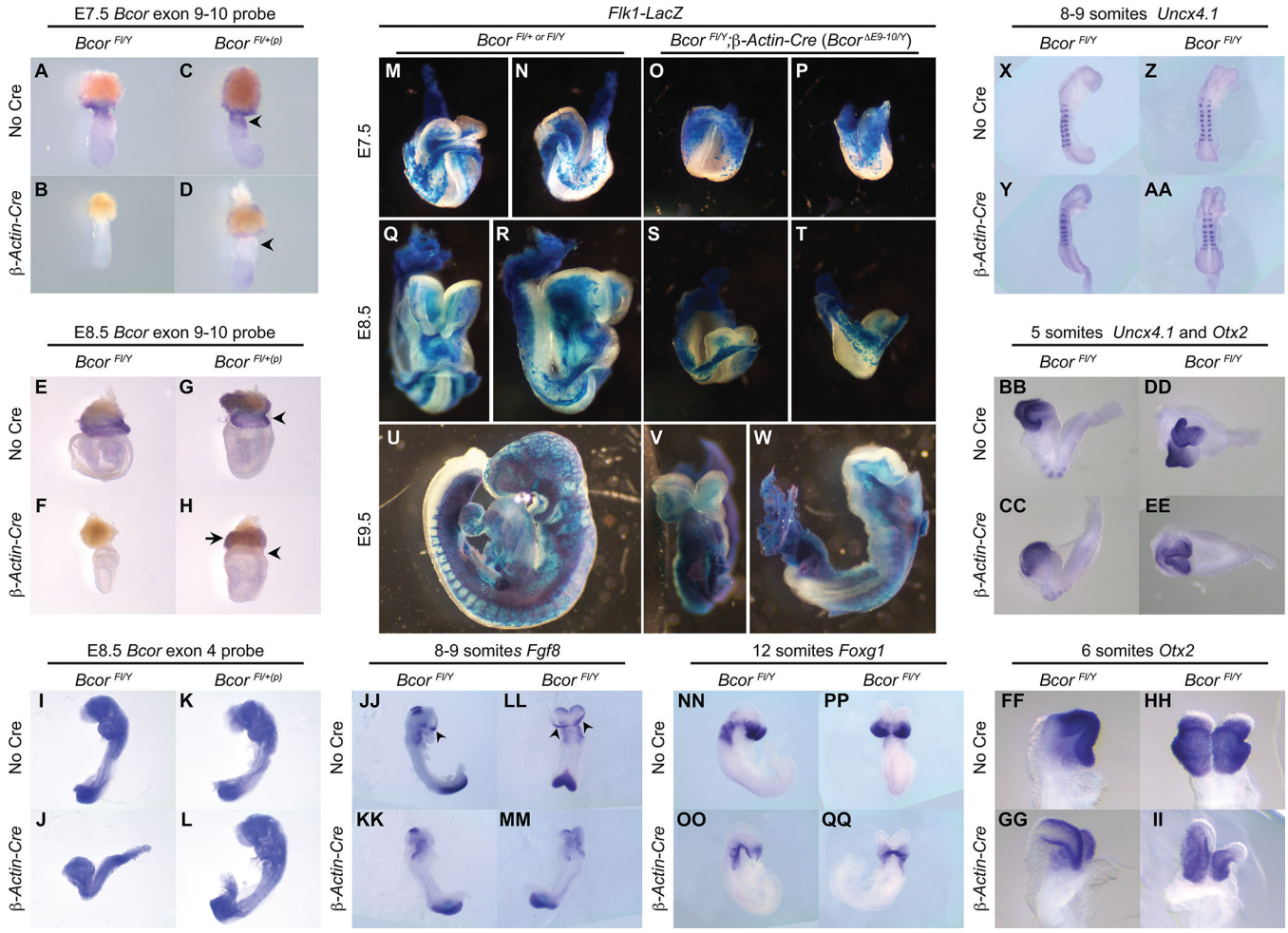

Figure 3. Early embryonic lethality in *Bcor* $^{\Delta E9-10/Y}$ males.

(A-L) *Bcor in situ* analysis using probe sequences absent (exon 9–10, A-H) or present (exon 4, I-L) in the deleted allele. The exon 4 probe is more robust and is able to maintain hybridization with the exon 9–10 deleted transcript. Arrowheads indicate extra-embryonic ectoderm/chorionic region; arrow indicates escape from paternal XCI in P-TGCs. (M-W) LacZ staining in *Flk1* expressing lineages of early embryonic development for control (M, N, Q,R, U) and *Bcor* $^{\Delta E9-10/Y}$ (O, P, S, T, V, W) embryos. (X-II) *In situ* analysis in somite-number matched control (X, Z, BB, DD, FF, HH, JJ, LL, NN and PP) and *Bcor* $^{\Delta E9-10/Y}$ embryos (Y, AA, CC, EE, GG, II, KK, MM, OO and QQ) showing *Uncx2.1*, a marker of somites (X-EE), *Otx2*, a marker of forebrain and midbrain (BB-II), *Fgf8* a marker of the anterior neural ridge (JJ-MM, arrowhead) and *Foxg1* a marker of forebrain (NN-QQ).

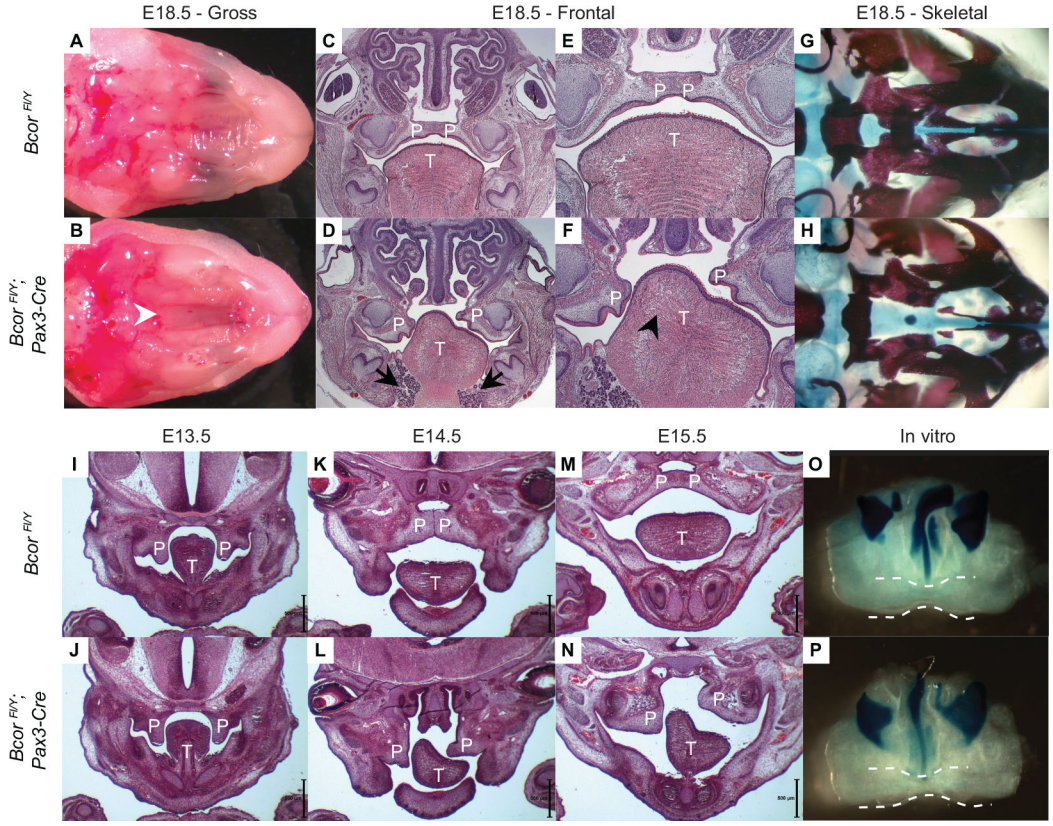

Figure 4. *Bcor* is required in neural crest lineages outside the palate for normal palate formation.

(A, B) E18.5 gross morphology of the maxillary region (mandibles removed) in control *Bcor* $^{Fl/Y}$ (A) and mutant, *Bcor* $^{Fl/Y}$;*Pax3-Cre* (B), which has cleft palate (white arrow head). Clefting was observed in all mutants (n>10). (C-F) H & E staining of frontal sections through E18.5 heads confirms the cleft palate in mutant (D, expanded in F) but not in control (C, expanded in E). In addition, mutants had ectopic salivary glands in the submandibular region (D, black arrows) and disorganized tongue morphology (F, black arrowhead). Both phenotypes were present in all mutants examined (n>4). P = palatal shelves, T = tongue. (G-H) Skeletal preparations of E18.5 control *Bcor* $^{Fl/Y}$ (G), and mutant *Bcor* $^{Fl/Y}$;*Pax3-Cre,* (H) heads, mandibles removed, confirm cleft palate defect. Cartilage is stained with Alcian blue, while bone is stained with Alizarin red. These phenotypes were observed in all mutant skeletal preparations (n=3). (I-N) Time course of palatal shelf elevation. H & E staining of frontal sections through *Bcor* $^{Fl/Y}$ control (I, K, M) and *Bcor* $^{Fl/Y}$;*Pax3-Cre* mutant (J, L, N) palates at indicated ages reveals a failure in palatal shelf elevation that became evident at E14.5 and persisted throughout development. Scale bars, 0.5 mm. These phenotypes were observed in all mutants (n=2 for each time point). (O,P) *Bcor* mutant palatal shelves can elevate and fuse in culture. Alcian blue staining of cartilaginous structures in *Bcor* $^{Fl/Y}$ control (O) and *Bcor* $^{Fl/Y}$;*Pax3-Cre* mutant (P) palatal shelves isolated at E12.5, cultured for 5 days and cartilage stained with Alcian blue. Dashed white lines outline the elevated and fused palate in both the control and the mutant tissue.

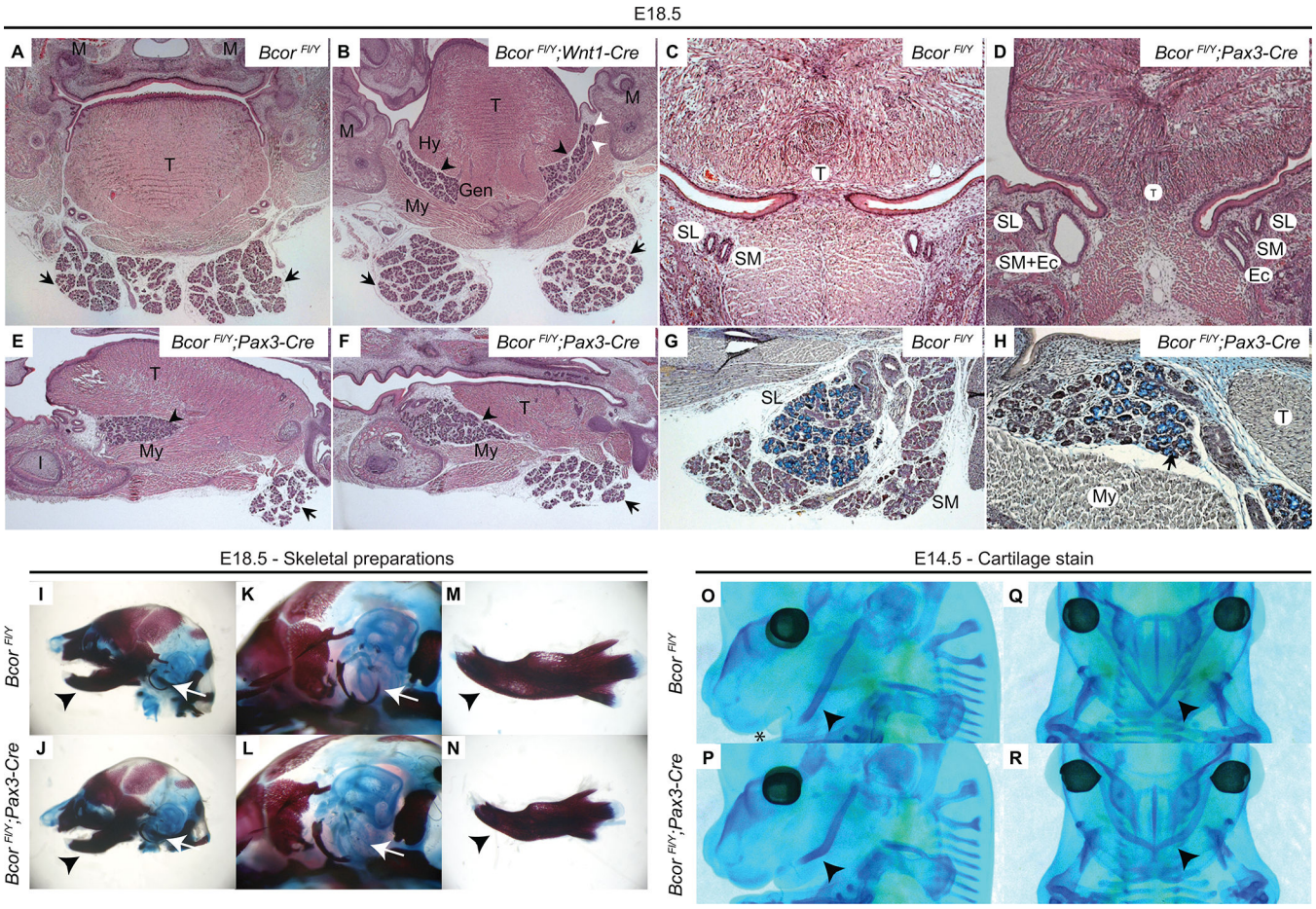

Figure 5. *Bcor* is required in neural crest lineages to suppress ectopic salivary gland formation and for normal craniofacial development.

(A-F) H & E stained frontal (A-D) and sagittal (E, F) sections through control *Bcor* $^{FL/Y}$ (A, C), *Bcor* $^{FL/Y}$;*Wnt1-Cre* (B), and *Bcor* $^{FL/Y}$;*Pax3-Cre* (D, E, F) E18.5 heads. (A) In control animals, two pairs of, submandibular and sublingual salivary glands (arrows) are found below the lower jaw in control animals. (B) In the mutant, in addition to the normal pairs of SM and SL glands (arrows), an ectopic pair of salivary glands (black arrowheads) is found between the mylohyoid, hyoglossus, and genioglossus muscles. Main excretory ducts of the SM and SL glands also run through this area on the buccal side (white arrowheads). (A) and (B) are sectioned at the level of the first molars (M). (C) In control animals two excretory ducts are found on each side of the lower jaw, the SL duct on the buccal side and the SM duct on the lingual side. (D) In mutant animals, excretory ducts of ectopic SGs run alongside the ones of the SL and SM glands, on the lingual side. They are either completely separate ducts (right hand side) or join with the SM duct shortly before it opens in the mouth (left hand side). (E) At the midline, ectopic SGs (arrowhead) abut the lingual frenulum. (F) Further from the midline, on the buccal side of the tongue, ectopic (arrowhead) and regular (arrow) SGs come closer to each other. (F) Ectopic SGs (arrowhead) are positioned more distally along the proximo-distal axis of the lower jaw than the SM and SL glands (arrow). (G, H) Trichrome-stained sagittal sections through *Bcor* $^{FL/Y}$ (G) and *Bcor* $^{FL/Y}$;*Pax3-Cre* (H) E18.5 heads. Groups of mucous acini stained in blue (black, arrow) are found on the

buccal side of ectopic SGs (H), reminiscent of the SL gland in control animals (G). Ec = ectopic salivary gland, Gen = genioglossus muscle, Hy = hyoglossus muscle, I = lower incisor, M = first molar, My = mylohyoid muscle, SL = sublingual salivary gland, SM = submandibular salivary gland, T = tongue. (I-N) Skeletal preparations of E18.5 control *Bcor* $^{Fl/Y}$ (I, K, M) and mutant *Bcor* $^{Fl/Y}$;*Pax3-Cre* (J, L, N) heads reveal shortening of the tympanic ring bone (white arrows indicate the normal position of the dorsal end; I, K vs. J, L) and mandible (black arrowheads, I, M vs. J, N). Cartilage is stained with Alcian blue and bone is stained with Alizarin red. These phenotypes were observed in all mutants (n=7). (O-R) Alcian blue staining of cartilaginous structures in E14.5 *Bcor* $^{Fl/Y}$ control (O, Q) and *Bcor* $^{Fl/Y}$;*Pax3-Cre* mutant (P, R) mice reveals defective Meckel's cartilage patterning in the mutant animals, in side (O, P) and frontal (Q, R) views (black arrowheads). Note tongue protrudes from mouth in control (asterisk) but not mutant. These phenotypes were observed in all mutants (n=9).

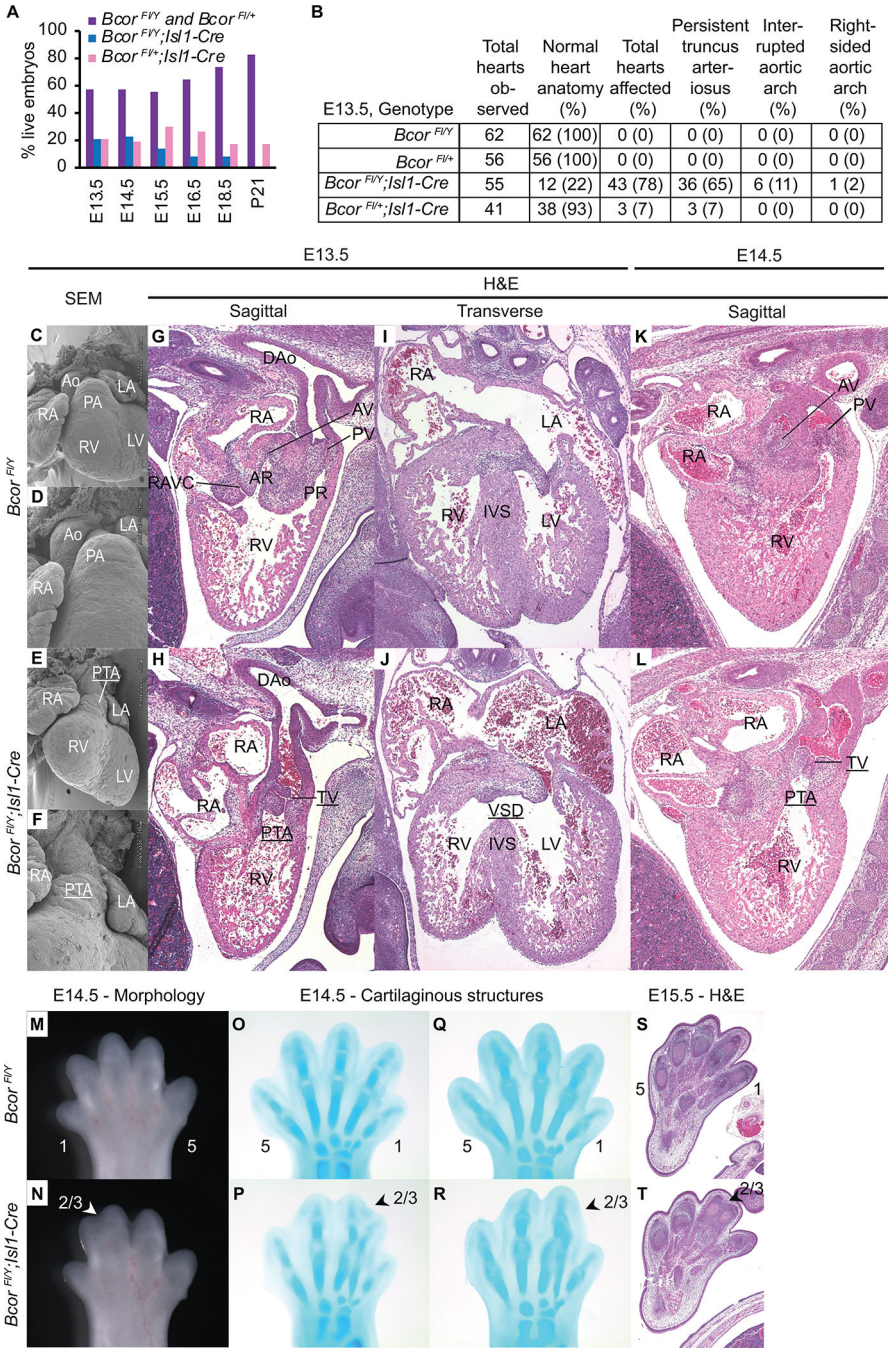

E13.5, Genotype	Total hearts observed	Normal heart anatomy (%)	Total hearts affected (%)	Persistent truncus arteriosus (%)	Interrupted aortic arch (%)	Right-sided aortic arch (%)
Bcor $^{Fl/Y}$	62	62 (100)	0 (0)	0 (0)	0 (0)	0 (0)
Bcor $^{Fl/+}$	56	56 (100)	0 (0)	0 (0)	0 (0)	0 (0)
Bcor $^{Fl/Y}$;*Isl1-Cre*	55	12 (22)	43 (78)	36 (65)	6 (11)	1 (2)
Bcor $^{Fl/+}$;*Isl1-Cre*	41	38 (93)	3 (7)	3 (7)	0 (0)	0 (0)

Figure 6. *Bcor* is required in *Isl1*-expressing cell lineages for normal cardiac outflow tract formation and ventricular septation and hindlimb patterning.

(A) Survival/Lethality of E13.5 (n=263), E14.5 (n=30), E15.5 (n=42), E16.5 (n=26), E18.5 (n=35) and P21 (n=39) animals. Cardiac analysis (B-L): Summary of visible cardiac defects at E13.5 (B). (C-F) Scanning electron microscopy of *Bcor* $^{Fl/Y}$ (C, D) and *Bcor* $^{Fl/Y}$;*Isl1-Cre* (E, F) hearts at E13.5 reveals persistent truncus arteriosus (PTA) in mutant hearts. (G - L) H & E staining of *Bcor* $^{Fl/Y}$ (G, I, K), and *Bcor* $^{Fl/Y}$; *Isl1-Cre* (H, J, L) hearts at E13.5 (G-J) and E14.5 (K-L) sections confirm PTA in the mutant hearts (H, L) and illustrate ventricular septal defect (J) compared to control (G, I, K) Ao = aorta, PA = pulmonary artery, RA =

right atrium, LA = left atrium, RV = right ventricle, LV = left ventricle, DAo = descending aorta, AR = aortic root, PR = pulmonary root, RAVC = right atrioventricular canal, PTA = persistent truncus arteriosus, PT = truncal valve, VSD = ventricular septal defect. (M-T) Hindlimb analysis: Gross morphology (M, N) and Alcian blue staining (O-R) of hindlimbs at E14.5 in *Bcor* $^{Fl/Y}$ (M, O, Q) and *Bcor* $^{Fl/Y}$; *Isl1-Cre* (N, P, R) and H & E staining of *Bcor* $^{Fl/Y}$ (S) and *Bcor* $^{Fl/Y}$; *Isl1-Cre* (T) E15.5 section showing mutants with second-third digit syndactyly (2/3 arrow heads).

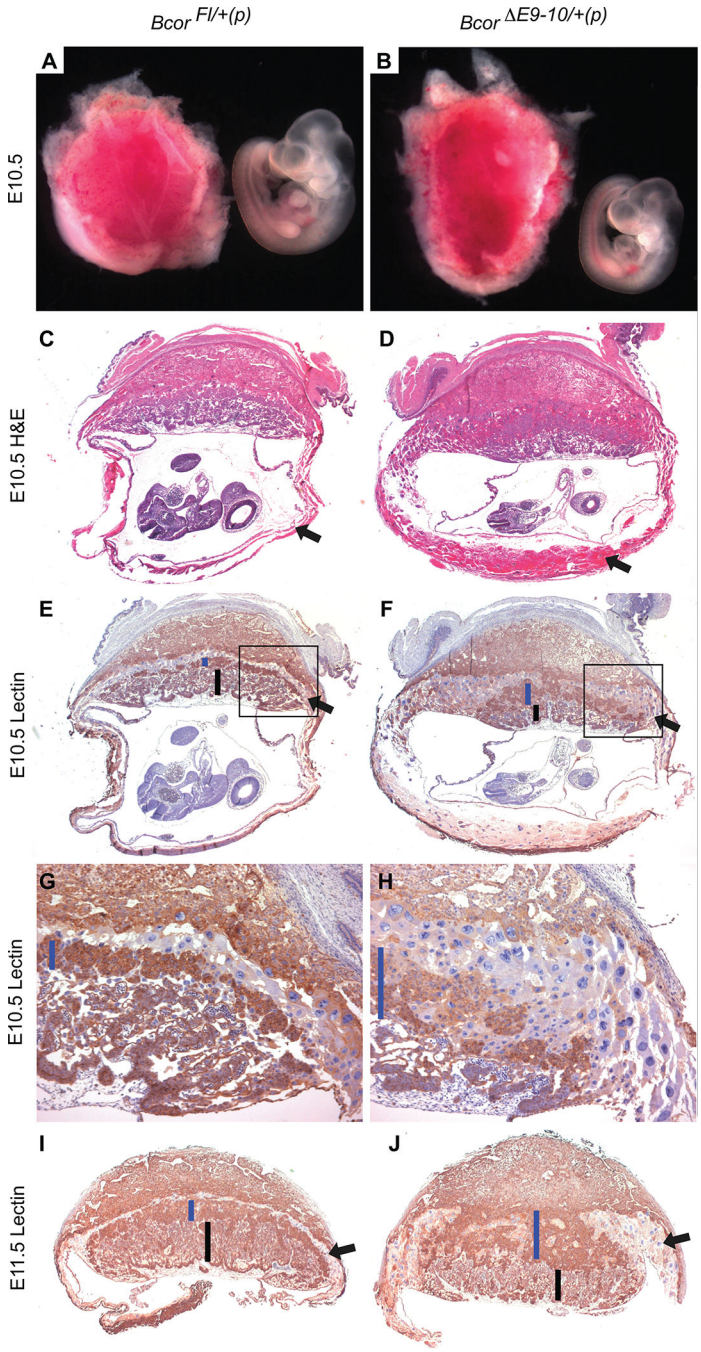

Figure 7: *Bcor* is required in extraembryonic lineages for placental development and consequently embryo survival.

(A,B) Freshly dissected E10.5 placentae and embryos illustrating IUGR and excess blood in *Bcor* $^{\Delta E9-10/+(p)}$ concepti (B) vs. *Bcor* $^{Fl/+(p)}$ control (A). Midpoint sections of E10.5 concepti (C-H) and E11.5 placentae (I, J) H & E (C,D) or lectin staining (E-J) of *Bcor* $^{Fl/+(p)}$ controls (C, E, G and I) vs. *Bcor* $^{\Delta E9-10/+(p)}$ (D,F,H, and J) showing P-TGC and Sp-T (blue line) cell expansion, reduced labyrinth (black line) and excess blood (bright pink) in mutants. Boxes in E and F indicate region expanded in G and H respectively.

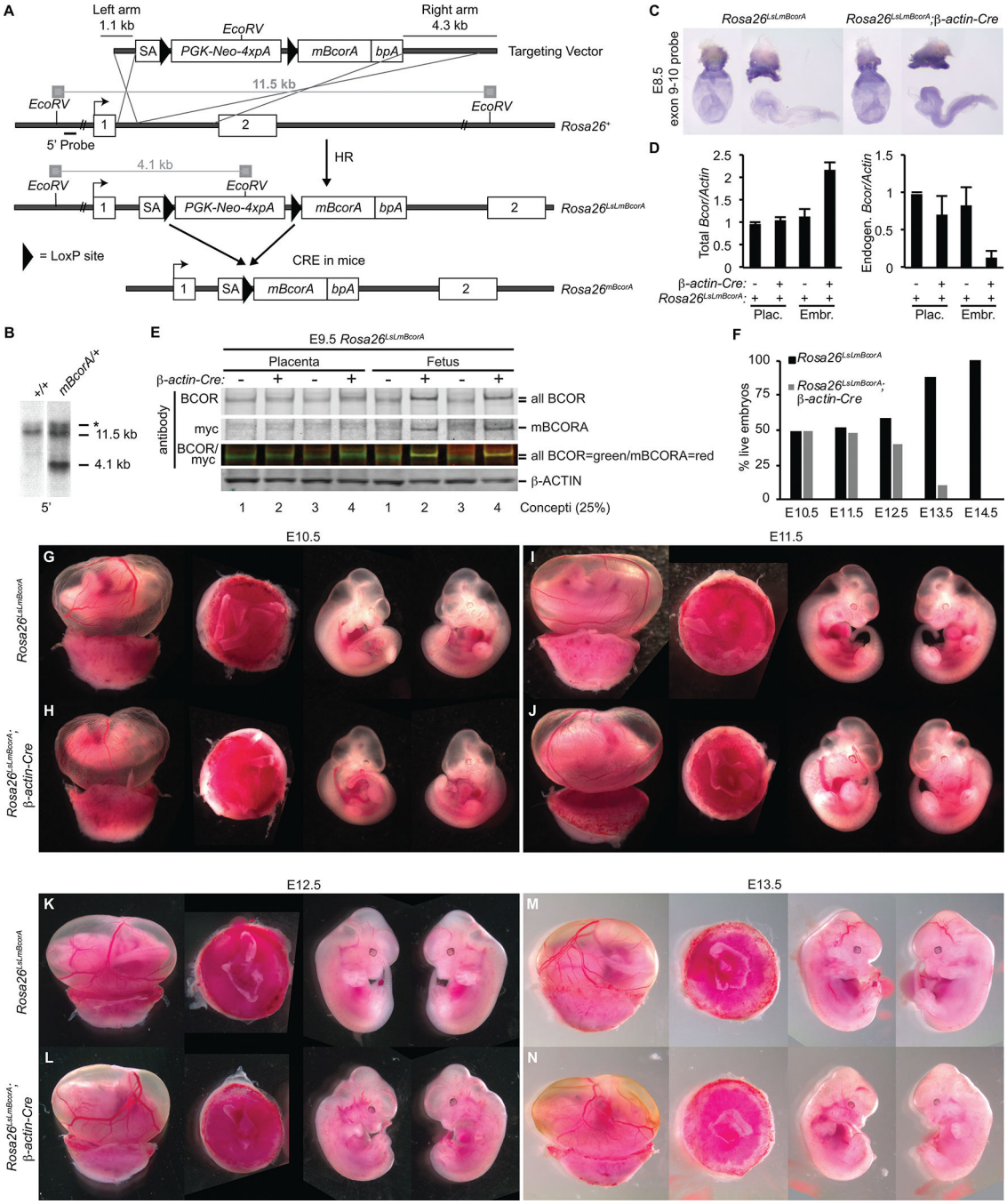

Figure 8: Generation and lethality of a conditional *Bcor* expression allele.

(A) Diagram of the targeting strategy. Homologous recombination in embryonic stem cells (ES cells) generated the *Rosa26*^{LsLmBcorA} allele, in which a splice acceptor (SA) site precedes a LoxP-flanked transcriptional "4xpA stop" sequence (4 copies of a polyadenylation signal) that is followed by a myc-tagged (m) murine *BcorA* (isoform A) coding sequence. CRE-mediated recombination excises the LoxP-flanked "stop" sequence, allowing expression of *myc-tagged BcorA* driven by the *Rosa26* promoter. (B) Southern blot hybridization of the wild type and targeted ES cell genomic DNA digested with *Eco*RV

reveals successful homologous recombination of the 5' homology arm. The introduced *Eco*RV site generates a 4.1 kb fragment in addition to the 11.5 kb band from the wild type allele (3' homology arm not shown). * = partially digested DNA. (C) In situ analysis of *Bcor* expression in $Rosa26^{LsLmBcorA/+}$ vs. $Rosa26^{mBcorA/+}$ concepti at E8.5. (D) quantitative RT-PCR comparing total *Bcor* transcripts (endogenous plus transgene, left) vs. endogenous (right) in $Rosa26^{LsLmBcorA/+}$ and $Rosa26^{mBcorA/+}$ placenta and embryos at E9.5. (E) Western blots of total BCOR levels vs. transgene expressed mBCORA in individual E9.5 fetuses (#1–4) and their placenta. In the color panel a yellow band corresponds to a protein stained with both BCOR and myc antibodies. (F) Survival of $Rosa26^{LsLmBcorA/+}$ vs. $Rosa26^{mBcorA/+}$ embryos from E10.5 (n=54), E11.5 (n=86), E12.5 (n=27), E13.5 (n=18) to E14.5 (n=9). (G-N) Images of representative $Rosa26^{LsLmBcorA/+}$ (G, I, K, M) and $Rosa26^{mBcorA/+}$ (H, J, L, N) placentae and embryos from E10.5 (G, H), E11.5 (I, J), E12.5 (K, L) and E13.5 (M, N) illustrating embryo phenotypes.